

<b>Title</b>	Formulation and evaluation of anisamide-targeted amphiphilic cyclodextrin nanoparticles to promote therapeutic gene silencing in a 3D prostate cancer bone metastases model
<b>Author(s)</b>	Evans, James C.; Malhotra, Meenakshi; Fitzgerald, Kathleen A.; Guo, Jianfeng; Cronin, Michael F.; O'Brien, Fergal J.; Curtin, Caroline M.; Darcy, Raphael; O'Driscoll, Caitríona M.
<b>Publication date</b>	2016-11-11
<b>Original citation</b>	Evans, J. C., Malhotra, M., Fitzgerald, K. A., Guo, J., Cronin, M. F., Curtin, C. M., O'Brien, F. J., Darcy, R. and O'Driscoll, C. M. (2016) 'Formulation and evaluation of anisamide-targeted amphiphilic cyclodextrin nanoparticles to promote therapeutic gene silencing in a 3D prostate cancer bone metastases model', <i>Molecular Pharmaceutics</i> , 14(1), pp. 42-52. doi:10.1021/acs.molpharmaceut.6b00646
<b>Type of publication</b>	Article (peer-reviewed)
<b>Link to publisher's version</b>	<a href="http://dx.doi.org/10.1021/acs.molpharmaceut.6b00646">http://dx.doi.org/10.1021/acs.molpharmaceut.6b00646</a> Access to the full text of the published version may require a subscription.
<b>Rights</b>	© 2016, American Chemical Society. This document is the Accepted Manuscript version of a Published Work that appeared in final form in <i>Molecular Pharmaceutics</i> , after peer review and technical editing by the publisher. To access the final edited and published work see <a href="http://pubs.acs.org/doi/abs/10.1021/acs.molpharmaceut.6b00646">http://pubs.acs.org/doi/abs/10.1021/acs.molpharmaceut.6b00646</a>
<b>Embargo information</b>	Access to this article is restricted until 12 months after publication by request of the publisher.
<b>Embargo lift date</b>	2017-11-11
<b>Item downloaded from</b>	<a href="http://hdl.handle.net/10468/4411">http://hdl.handle.net/10468/4411</a>

Downloaded on 2018-08-23T18:26:25Z

## Formulation and evaluation of anisamide-targeted amphiphilic cyclodextrin nanoparticles to promote therapeutic gene silencing in a 3D prostate cancer bone metastases model

James C Evans, Meenakshi Malhotra, Kathleen A Fitzgerald, Jianfeng Guo, Michael F Cronin, Caroline M Curtin, Fergal J O'Brien, Raphael Darcy, and Caitriona M O'Driscoll

*Mol. Pharmaceutics*, **Just Accepted Manuscript** • DOI: 10.1021/acs.molpharmaceut.6b00646 • Publication Date (Web): 11 Nov 2016

Downloaded from <http://pubs.acs.org> on November 16, 2016

### Just Accepted

"Just Accepted" manuscripts have been peer-reviewed and accepted for publication. They are posted online prior to technical editing, formatting for publication and author proofing. The American Chemical Society provides "Just Accepted" as a free service to the research community to expedite the dissemination of scientific material as soon as possible after acceptance. "Just Accepted" manuscripts appear in full in PDF format accompanied by an HTML abstract. "Just Accepted" manuscripts have been fully peer reviewed, but should not be considered the official version of record. They are accessible to all readers and citable by the Digital Object Identifier (DOI®). "Just Accepted" is an optional service offered to authors. Therefore, the "Just Accepted" Web site may not include all articles that will be published in the journal. After a manuscript is technically edited and formatted, it will be removed from the "Just Accepted" Web site and published as an ASAP article. Note that technical editing may introduce minor changes to the manuscript text and/or graphics which could affect content, and all legal disclaimers and ethical guidelines that apply to the journal pertain. ACS cannot be held responsible for errors or consequences arising from the use of information contained in these "Just Accepted" manuscripts.



**Formulation and evaluation of anisamide-targeted amphiphilic cyclodextrin nanoparticles to promote therapeutic gene silencing in a 3D prostate cancer bone metastases model**

**Authors**

James C. Evans<sup>1</sup>

Meenakshi Malhotra<sup>1</sup>

Kathleen A. Fitzgerald<sup>1</sup>

Jianfeng Guo<sup>1</sup>

Michael F. Cronin<sup>1</sup>

Caroline M. Curtin<sup>2</sup>

Fergal J O'Brien<sup>2</sup>

Raphael Darcy<sup>1</sup>

Caitriona M O'Driscoll<sup>1</sup>

<sup>1</sup>Pharmacodelivery Group, School of Pharmacy, University College Cork, Cork, Ireland.

<sup>2</sup>Tissue Engineering Research Group, Anatomy Department, Royal College of Surgeons in Ireland, Dublin, Ireland; Trinity Centre for Bioengineering, Trinity College, Dublin, Ireland; Advanced Materials and Bioengineering Research (AMBER) Centre, RCSI & TCD, Ireland.

All correspondence relating to this paper should be addressed to:

Professor Caitriona O'Driscoll,

School of Pharmacy,

University College Cork,

Ireland.

Tel: +353-21-4901396

Fax: +353-21-4901656

E-mail:caitriona.odriscoll@ucc.ie

**Abstract**

In recent years, RNA interference (RNAi) has emerged as a potential therapeutic offering the opportunity to treat a wide range of diseases, including prostate cancer. Modified cyclodextrins have emerged as effective gene delivery vectors in a range of disease models. The main objective of the current study was to formulate anisamide-targeted cyclodextrin nanoparticles to interact with the sigma receptor (overexpressed on the surface of prostate cancer cells). The inclusion of octaarginine in the nanoparticle optimised uptake and endosomal release of siRNA in two different prostate cancer cell lines (PC3 and DU145 cells). Resulting nanoparticles were less than 200 nm in size with a cationic surface charge (~+20 mV). In sigma receptor-positive cell lines, the uptake of anisamide-targeted nanoparticles was reduced in the presence of the sigma receptor competitive ligand, haloperidol. When cells were transfected in 2D, the levels of PLK1 mRNA knockdown elicited by targeted versus untargeted nanoparticles tended to be greater but the differences were not statistically different. In contrast, when cells were grown on 3D scaffolds, recapitulating bone metastasis, targeted formulations showed significantly higher levels of PLK1 mRNA knockdown (46 % for PC3 and 37 % for DU145,  $p < 0.05$ ). To our knowledge, this is the first time that a targeted cyclodextrin has been used to transfect prostate cancer cells in a 3D model of bone metastasis.

Keywords: RNAi, Sigma receptor, prostate cancer metastasis, collagen scaffolds, siRNA delivery, bone microenvironment

## Introduction

Prostate cancer is the most commonly diagnosed non-cutaneous cancer in men of the western world <sup>1</sup>, with approximately 220,000 newly diagnosed cases and 28,000 deaths in the USA alone in 2015 <sup>2</sup>. The vast majority of prostate cancer cases are diagnosed at the local stage, where many effective and curative options are available (including surgery and radiotherapy) <sup>3</sup>. However, when the disease becomes metastatic, it is far more difficult to treat, with newly developed drugs (such as Cabazitaxel and Abiraterone Acetate) offering only a very modest increase in the length of survival (approximately 2.4 to 4.8 months) <sup>4, 5</sup>. Hence new treatments are urgently required.

RNA interference (RNAi) occurs in the majority of eukaryotic cells where double stranded RNA (dsRNA) regulates gene expression in a sequence-specific manner <sup>6</sup>. Fire and Mello were awarded the Nobel Prize in 2006 for this discovery and it opened up the potential of using RNAi to treat a wide range of diseases including cancer <sup>7</sup>. However, the development of RNAi drugs has been slow, with the key obstacle to clinical translation being the design of an effective delivery vector that is capable of binding, protecting and efficiently delivering siRNA to the target tissue <sup>8</sup>.

Cyclodextrins (CD) are naturally occurring cyclic oligosaccharides that are formed by the enzymatic degradation of starch <sup>9</sup>. Modified CDs used for siRNA delivery have been shown to effectively facilitate gene silencing in a wide range of disease models including Huntington's disease, inflammatory bowel disease (IBD) and prostate cancer <sup>10-13</sup>.

The sigma receptor is a membrane bound protein that is known to be overexpressed in a wide range of human cancers, including prostate cancer <sup>14</sup>. Recently, our group developed a modified CD with a guanidino group on the primary-OH face to complex siRNA and an anisamide group (a ligand for the sigma receptor) on the secondary-OH face to target the

1  
2  
3 delivery vector to prostate cancer cells. The anisamide-targeted CD successfully silenced  
4  
5 VEGF mRNA in PC3 prostate cancer cells and significantly reduced tumour volume in a  
6  
7 TRAMP-C1 induced xenograft mouse model of prostate cancer, following its intravenous  
8  
9 administration <sup>15</sup>. In addition, we have also shown that the anisamide targeting ligand can be  
10  
11 incorporated into hydrophilic dilysine-CD nanoparticles by inclusion complex formation  
12  
13 achieved by attaching the ligand via a PEG chain to adamantane; a hydrophobic molecule  
14  
15 known to form stable inclusion complexes with cyclodextrins <sup>16</sup>. This formulation produced  
16  
17 high levels of anisamide-mediated cellular uptake but modest levels of gene silencing.  
18  
19

20  
21 Octaarginine (R8) is a cell penetrating peptide (CPP). CPPs are typically less than 30 amino  
22  
23 acid residues in length and rich in lysine and/or arginine. The highly cationic nature of these  
24  
25 peptides aids cellular uptake and also enhances endosomal escape <sup>17</sup>. Recently, post-insertion  
26  
27 of DSPE-PEG<sub>2000</sub>-R8 into preformed CD.siRNA nanoparticles resulted in a greater level of  
28  
29 knockdown in mHypoE N41 cells when compared to both CD.siRNA alone and a PEGylated  
30  
31 control <sup>18</sup>.  
32  
33

34  
35 Traditionally when developing novel therapeutics to treat cancer, *in vitro* studies are carried  
36  
37 out on cells grown in a monolayer. This approach, while useful, has several limitations  
38  
39 highlighting the advantages of developing three dimensional (3D) cell culture models to  
40  
41 simulate the physiological microenvironment <sup>19-21</sup>. Recently, a 3D model of prostate cancer  
42  
43 bone metastasis was established by culturing LNCaP and PC3 prostate cancer cells on  
44  
45 collagen-based scaffolds engineered to mimic the bone microenvironment. Cells cultured in  
46  
47 3D were successfully transfected with CD.siRNA nanoparticles and demonstrated high levels  
48  
49 of siRNA uptake and highly efficient gene silencing <sup>22</sup>. As the bone is the major site of  
50  
51 secondary metastases in prostate cancer and negatively impacts a patient's quality of life due  
52  
53 to pain, fractures and spinal cord and nerve root compression, this 3D pre-clinical bone model  
54  
55 could provide a useful biopharmaceutical tool to help develop and evaluate novel therapies <sup>23</sup>,  
56  
57  
58  
59  
60

1  
2  
3 24. Physiologically relevant 3D models of disease facilitate mechanistic studies at the cellular  
4  
5 level and can help predict the *in vivo* response, thus improving *in vitro-in vivo* correlations  
6  
7 while simultaneously reducing the number of live animal experiments in accordance with the  
8  
9 three R's principle 25.  
10

11  
12 The aim of the current study was to formulate a multifunctional anisamide-targeted CD  
13  
14 nanoparticle containing the R8 endosomal escape peptide to deliver therapeutic siRNA to  
15  
16 prostate cancer cells via binding to the sigma receptor. Where previously we had incorporated  
17  
18 the anisamide targeting ligand by exploiting CD inclusion complex formation 16, in this paper  
19  
20 a different formulation approach was investigated and the nanoparticles were formulated by  
21  
22 using post-insertion of DSPE-PEG<sub>5000</sub>-anisamide and DSPE-PEG<sub>2000</sub>-R8 into preformed  
23  
24 amphiphilic CD.siRNA complexes. The physicochemical properties and the receptor specific  
25  
26 uptake of the targeted nanoparticles were assessed, and the gene silencing efficacy was  
27  
28 evaluated using a 3D scaffold model of bone metastasis.  
29  
30  
31  
32  
33  
34  
35  
36  
37  
38  
39  
40  
41  
42  
43  
44  
45  
46  
47  
48  
49  
50  
51  
52  
53  
54  
55  
56  
57  
58  
59  
60

## Materials and methods

### Materials

Anisic acid and dicyclohexylcarbodiimide (DCC) were procured from Sigma-Aldrich (St Louis, MO, USA). DSPE-PEG<sub>5000</sub>-amine and DSPE-PEG<sub>5000</sub>-methyl (DPM) were purchased from Nanocs (New York, NY, USA). Slide-A-Lyzer Dialysis Cassettes (MWCO – 3.5 KDa) were purchased from Pierce-Thermo Scientific (Waltham, MA, USA). Heptakis[2-O-(N-(3''-aminopropyl)-1'H-triazole-4'-yl-methyl)-6-dodecylthio]- $\beta$ -cyclodextrin (**Figure 1**), the cationic amphiphilic cyclodextrin, was synthesized as previously described<sup>26</sup>.

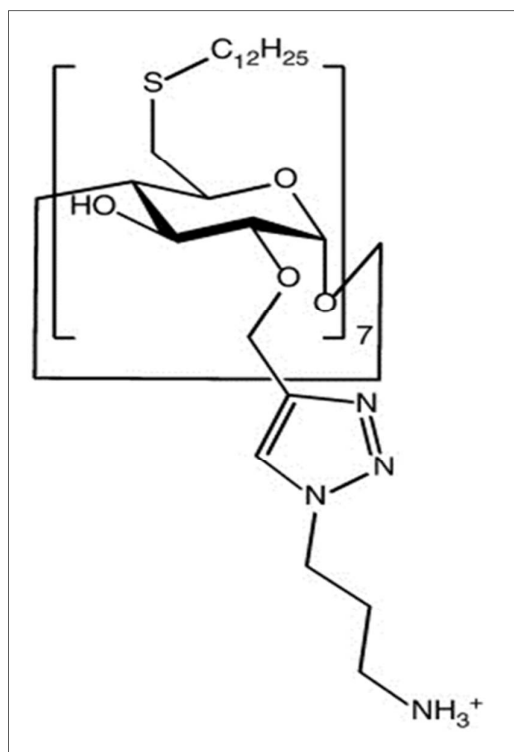


**Figure 1:** Chemical structure of the cationic amphiphilic cyclodextrin<sup>26</sup>.

### Synthetic siRNA

Synthetic siRNA duplexes were obtained from Sigma-Aldrich, IDT or Genepharma. Negative control siRNA and 6-carboxyfluorescein (6-FAM)-labelled negative control siRNA were



1  
2  
3 obtained from Sigma Aldrich (St. Louis, Missouri). Luciferase siRNA was custom  
4  
5 synthesized by IDT (Coralville, Iowa) with the following sequence: (sense 5'-  
6  
7 GGGGGACGAGGACGAGCACUTC-3'). PLK1 siRNA was synthesized by Genepharma  
8  
9 (Shanghai, China) with the following sequence: (sense 5'-  
10  
11 AGAmUCACCCmUCCUmUAAAmUAUU-3'), where "m" indicates a 2'-O-methylated  
12  
13 nucleotide on the right.  
14

#### 15 16 **Synthesis of DSPE-PEG<sub>5000</sub>-anistic acid**

17  
18  
19 P-anistic acid (5.26 mg, 0.0346 mmol) was dissolved in DMSO (2 ml). DSPE-PEG<sub>5000</sub>-Amine  
20  
21 (100 mg, 0.0173 mmol) was dissolved in pyridine (1 ml) and added to the anistic acid-DMSO  
22  
23 solution followed by the addition of DCC (16 mg, 0.7785 mmol). The reaction was carried  
24  
25 out at room temperature for 4 h. The solution was dialyzed in Slide-A-Lyzer Dialysis  
26  
27 Cassettes with a MWCO of 3.5 KDa against deionized water for 3 days. The dialysate was  
28  
29 further lyophilized and the final product was analyzed by FTIR and <sup>1</sup>H NMR.  
30  
31

#### 32 33 **Preparation of CD.siRNA nanoparticles**

34  
35  
36 Cyclodextrin was dissolved in chloroform to a final concentration of 1 mg /ml. Chloroform  
37  
38 was removed under a steady stream of nitrogen gas. The resulting lipid films were dissolved  
39  
40 in water to 1 mg /ml and were sonicated for 1 h to reduce particle size. To form CD.siRNA  
41  
42 nanoparticles, CD and siRNA were mixed at a specific mass ratio (in this case MR20) of CD  
43  
44 to siRNA. These were allowed to stabilize at room temperature for 20-30 minutes. A post-  
45  
46 insertion method was then used to insert PEG chains and R8 into CD.siRNA NPs. Briefly,  
47  
48 DSPE-PEG<sub>5000</sub>-anisamide, DSPE-PEG<sub>5000</sub>-methyl and DSPE-PEG<sub>2000</sub>-R8 were dissolved in  
49  
50 20mM HEPES buffer (pH 7.4) and heated at 37°C for 10 minutes. DSPE-PEG reagents were  
51  
52 mixed with CD.siRNA complexes which were heated at 37°C for 1 h at 300 rpm.  
53  
54  
55

#### 56 57 **Particle size and zeta potential (ζ)**

1  
2  
3 CD complexes were formed as detailed above and were made up to a final volume of 1 ml  
4  
5 with deionised (DI) water. Particle size and zeta potential were measured using a Malvern  
6  
7 Zeta Sizer (Malvern, Worcestershire, UK).  
8  
9

### 10 **Nanoparticle assessment in physiological conditions**

11  
12  
13 In order to determine the ability of the CD complexes to protect siRNA in the presence of  
14  
15 serum, complexes were incubated at 37°C for various time points (0, 5, 15, 60, 120, 240 and  
16  
17 480 mins). At each of the time points, complexes were heated at 80°C for 5 min followed by  
18  
19 incubation with excess heparin (5µl of a 2000U/ml solution, Sigma) for 1 h at room  
20  
21 temperature. Samples were run on a 1.5 % agarose gel at 120 V for 30 minutes. A salt  
22  
23 containing media (i.e. OptiMEM®) was used to determine the ability of the nanoparticles to  
24  
25 resist aggregation. Complexes were diluted to a final concentration of OptiMEM® of 90 %  
26  
27 v/v. At 4, 24 and 48 h aggregation was determined using the Malvern Zeta Sizer as above.  
28  
29  
30  
31

### 32 **Cell culture**

33  
34  
35 Luciferase cells stably transfected with the pGL4 Luc2 plasmid (Luc PC3) (donated by Dr  
36  
37 Coulter, School of Pharmacy, Queens University Belfast, Belfast, NI) and DU145 cells  
38  
39 (donated by Professor Watson, Conway Research Institute, University College Dublin,  
40  
41 Dublin, Ireland) were maintained in RPMI 1640 medium supplemented with 10 % FBS, 2  
42  
43 mM L-Glutamine and 50 units/ml penicillin and 50 µg/ml streptomycin. Mouse macrophage  
44  
45 RAW264.5 cells were maintained in Dulbecco's Modified Eagle's Medium supplemented  
46  
47 with 10 % FBS and 50 units/ml penicillin and 50 µg/ml streptomycin. All cells were grown in  
48  
49 the Forma Series II Water Jacketed CO<sub>2</sub> incubator (Thermo Electron Corporation, Waltham,  
50  
51 Massachusetts) at 37°C with 5 % CO<sub>2</sub> and 95 % relative humidity.  
52  
53  
54

### 55 **MTT assay**

1  
2  
3  $1 \times 10^4$  PC3 or DU145 cells were seeded into a 96 well plate 24 h prior to transfection. 100 nM  
4  
5 siRNA complexed with Lipofectamine 2000 (LF2000) or CD were prepared as above and  
6  
7 added to cells. After 24 h or 48 h, the complexes were removed and fresh serum-free media  
8  
9 supplemented with MTT reagent (5 mg/ml) was added and incubated for additional 4 h at  
10  
11  $37^\circ\text{C}$ . Following incubation, the resulting formazan crystals were dissolved in dimethyl  
12  
13 sulfoxide (DMSO). Absorbance was measured at 590 nm using a multiplate reader (Perkin  
14  
15 Elmer – Wallac Victor2™ 1420 multiplate counter).  
16  
17

### 18 19 **Cell culture in 3D on collagen-based scaffolds**

20  
21  
22 Collagen-nHA scaffolds (S500), containing 5-fold nanohydroxyapatite to collagen by weight,  
23  
24 were synthesised as previously described<sup>27</sup>. 24 h prior to transfection,  $1 \times 10^5$  PC3 or DU145  
25  
26 cells were seeded onto the scaffolds. Briefly,  $5 \times 10^4$  cells (in 25  $\mu\text{l}$  of media) were seeded  
27  
28 onto one side of the scaffold and left for 15 min at room temperature. Scaffolds were then  
29  
30 inverted and a further  $5 \times 10^4$  cells were seeded onto the opposite side of the scaffold.  
31  
32 Following this, 1 ml of complete media was added to each well and cells were incubated for  
33  
34 24 h at  $37^\circ\text{C}$  before performing further experiments.  
35  
36  
37

### 38 39 **Competitive uptake and uptake of targeted nanoparticles in 3D cell culture**

40  
41  
42 6-FAM-labelled scrambled siRNA was used for all uptake experiments. PC3 and DU145  
43  
44 cells ( $5 \times 10^4$ ) were seeded in 24-well plates, 24 h prior to transfection. 4 h prior to adding  
45  
46 complexes, cells were pre-treated with 40  $\mu\text{M}$  haloperidol (an antagonist of the sigma  
47  
48 receptor), 4 h later the media was replaced and 50 nM siRNA complexed with CD was added  
49  
50 to cells. After a further 4 h, the complexes were removed, the cells were washed twice with  
51  
52 PBS, lysed (in 1 % Triton X-100 and 2 % SDS) and protein concentrations were quantified  
53  
54 using a BCA assay<sup>28</sup>. Measurement of 6-FAM-labelled scrambled siRNA delivered by the  
55  
56 CD nanoparticles both in presence and absence of haloperidol was determined by measuring  
57  
58  
59  
60

1  
2  
3 the fluorescence intensity using a multiplate reader (excitation 485 nm, emission 535 nm) and  
4  
5 normalised to the protein content of the respective sample.  
6  
7

8 For visualization of siRNA delivered via CD nanoparticles to cell cultures in 3D, cells were  
9  
10 seeded onto the scaffolds as described above. 24 h after seeding, cells were transfected with  
11  
12 50 nM 6-FAM-labelled siRNA either alone or complexed in a targeted NP formulation. Ten  
13  
14 mins prior to imaging, cells were stained with 5 µg/mL solution of WGA-Alexa Fluor 633  
15  
16 (Invitrogen) prepared in Hank's Balanced Salt Solution at room temperature <sup>22</sup>. The 3D  
17  
18 scaffolds were imaged using an Olympus Fluoview FV1000 Laser Scanning Confocal  
19  
20 Microscope with IX71 microscope. Images were captured using Olympus FV10-ASW  
21  
22 software.  
23  
24  
25

### 26 **Luciferase assay**

27  
28  
29 PC3 cells ( $1 \times 10^4$ ) were seeded in white 24-well plates 24 h prior to transfection. Cells were  
30  
31 transfected with either LF2000 or CD complexed with 100 nM scrambled siRNA or  
32  
33 luciferase siRNA. 24 h later, complexes were removed and replaced with fresh media and  
34  
35 incubated for another 24 h. Following this time, media was replaced with fresh media  
36  
37 supplemented with D-Luciferin. The resulting luminescence was determined using a  
38  
39 multiplate reader at 560 nm and luminescence was normalised to protein concentration (using  
40  
41 BCA assay).  
42  
43  
44  
45

### 46 **RNAi transfection and Quantitative real-time (RT) PCR**

47  
48  
49 PC3 and DU145 cells ( $1 \times 10^5$ ) were seeded into 24-well plates 24 h prior to transfection.  
50  
51 Complexes were prepared as above and added to the cells at a final siRNA concentration of  
52  
53 100 nM. Complexes were removed 24 h later and incubated for an additional 24 h in fresh  
54  
55 media. Total RNA was extracted using the GenElute™ Mammalian Total RNA Mini-prep  
56  
57  
58  
59  
60

1  
2  
3 Kit (Sigma) and quantified using a Nanodrop (Thermo Fisher Scientific, Waltham, MA,  
4 USA). cDNA was synthesised using a High-capacity cDNA Reverse Transcription Kits  
5 (Applied Biosystems, Foster City, California). RT-PCR was performed using Applied  
6 Biosystems TaqMan® Gene expression assays for human PLK1 (catalogue number  
7 Hs00153444\_m1) and  $\beta$ -actin (catalogue number Hs01060665\_g1) and Applied Biosystems  
8 TaqMan® Universal PCR Master Mix. Quantitative real-time PCR was carried using the  
9 Applied Biosystems 7300 Real-Time PCR system. Cycling conditions were as follows: 10  
11 min at 95 °C, 40 cycles of [15 sec at 95 °C; 1 min at 60 °C]. Average cycle threshold (CT)  
12 values were used to determine gene expression.  $\beta$ -actin was used as an endogenous control  
13 and CT values were normalized to the levels of  $\beta$ -actin expression using the 2Delta CT  
14 method<sup>26</sup>.  
15  
16  
17  
18  
19  
20  
21  
22  
23  
24  
25  
26

### 27 28 **Pro-inflammatory cytokines**

29  
30  
31 RAW264.7 cells were seeded at  $1 \times 10^5$  cells per well in a 24 well plate, 24 h prior to  
32 transfection. Cells were incubated with LF2000 or CD complexes for 4 h or 24 h. LPS (10  
33 ng/ml) was used as a positive control for immunotoxicity as previously described<sup>10</sup>. RT-PCR  
34 was carried out as above using Applied Biosystems TaqMan® Gene expression assays for  
35 mouse  $\beta$ -actin (catalogue number 4352341E), COX-2 (catalogue number Mm00478374\_m1)  
36 and TNF- $\alpha$  (catalogue number Mm00443258\_m1).  
37  
38  
39  
40  
41  
42  
43  
44

### 45 **Statistical analysis**

46  
47  
48 Data were expressed as mean  $\pm$  standard deviation (SD). One-way Analysis of Variance  
49 (ANOVA) was used to test the significance of differences in three or more groups followed  
50 by Tukey's *post-hoc* test for all experiments except for **Figure 8** and **Figure 10**, where a two-  
51 tailed unpaired student *t*-test was used to compare PLK1 siRNA knockdown with its non-  
52 silencing counterpart. In all cases,  $P < 0.05$  was considered to be statistically significant  
53  
54  
55  
56  
57  
58  
59  
60

1  
2  
3 (\*p<0.05, p<0.01, \*\*\*p<0.001). All graphs and statistical calculations were prepared using  
4  
5 GraphPad Prism 5 (San Diego, California).  
6  
7  
8  
9  
10  
11  
12  
13  
14  
15  
16  
17  
18  
19  
20  
21  
22  
23  
24  
25  
26  
27  
28  
29  
30  
31  
32  
33  
34  
35  
36  
37  
38  
39  
40  
41  
42  
43  
44  
45  
46  
47  
48  
49  
50  
51  
52  
53  
54  
55  
56  
57  
58  
59  
60

## Results and discussion

In this study, four different cyclodextrin formulations were investigated as follows:

- 1) Formulation one was a cationic amphiphilic CD complexed with siRNA (hereafter referred to as CCD).
- 2) Formulation two was a targeted NP containing CCD co-formulated with a blend of DSPE-PEG<sub>5000</sub>-anisamide (DPAA) and DSPE-PEG<sub>2000</sub>-R8 (referred to as TR8+). Octaarginine (R8) was incorporated as it is a well-established endosomal escape peptide previously shown to have superior activity compared to other CPPs such as octalysine (K8)<sup>29</sup>.
- 3) Formulation three was a targeted NP but without R8 and contained CCD with DPAA only (referred to as TR8-).
- 4) Formulation four was the untargeted control NP containing CCD with DSPE-PEG<sub>5000</sub> (DPM) and DSPE-PEG<sub>2000</sub>-R8 (referred to as UR8+).

The exact composition of each of these formulations is given in **table 1**.

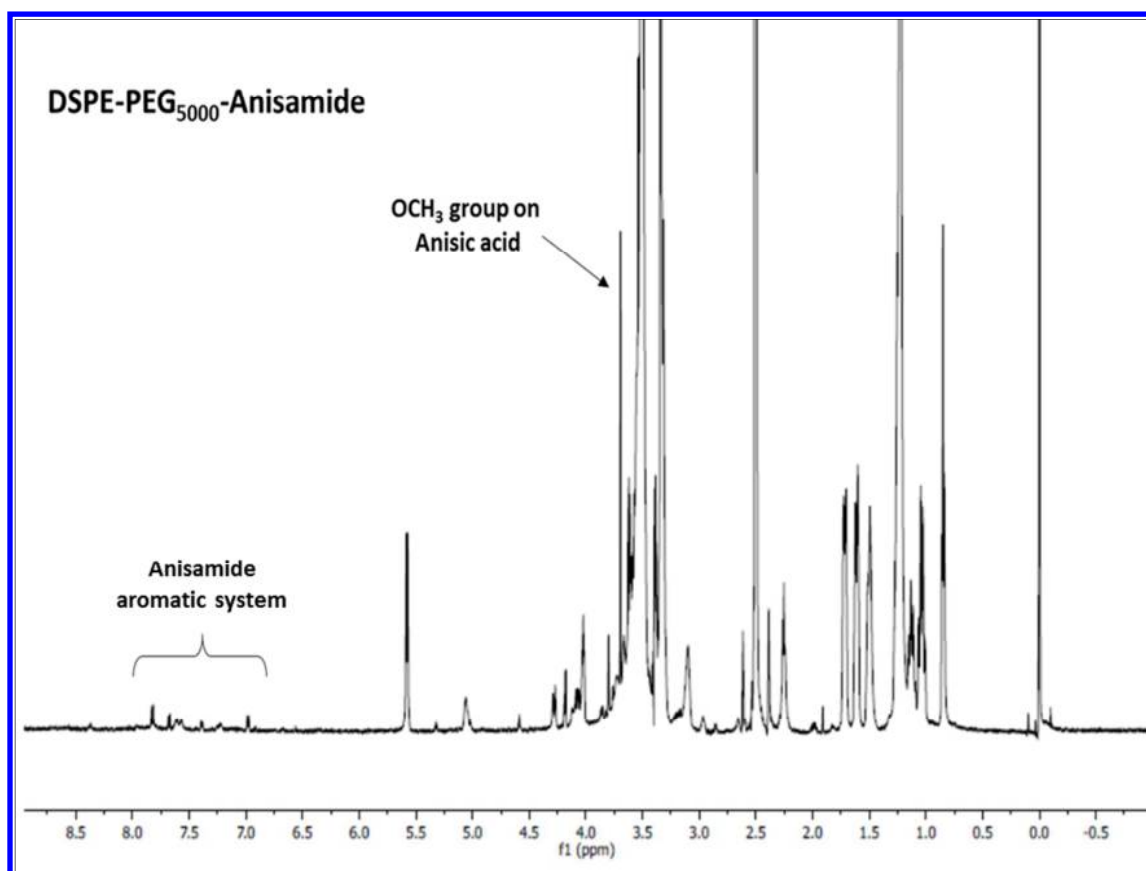
### Synthesis of DSPE-PEG<sub>5000</sub>-anisamide

DSPE-PEG<sub>5000</sub>-anisamide was synthesised as outlined above and the structure was verified by NMR and FTIR as indicated below (**Figures 2 and 3**).

### <sup>1</sup>H NMR analysis

<sup>1</sup>H NMR (600MHz, DMSO D<sub>6</sub>) δ0.85 (S, 6H, CH<sub>3</sub> x2), δ0.85 (S, 6H, CH<sub>3</sub> x2, alkyl chain termini), δ1.0-1.4 (M, 60H, CH<sub>2</sub> x 30, alkyl chain DSPE), δ1.5 (M, 4H, CH<sub>2</sub>CO x2, DSPE), δ3.0-4.3 (M, 453H, CH<sub>2</sub>O/CHO/CH<sub>2</sub>N, DSPE-PEG), δ3.8 (S, no integration, OCH<sub>3</sub>, anisic acid), δ5.0 (br S, 2H, NH x2), δ7.0 (d, J=12Hz, 0.24H, Ar-H, anisic acid), δ7.8 (d, J=12Hz, 0.24H, Ar-H, anisic acid). The integration performed by NMR analysis confirmed 12%

1  
2  
3 substitution of Anisic acid to DSPE-PEG-amine (**Figure 2**). This compound was further co-  
4  
5 formulated with nanoparticles as a targeting ligand and used for *in vitro* studies.  
6  
7



36  
37 **Figure 2:** <sup>1</sup>H NMR spectra of the conjugated DSPE-PEG5000 with AA in d<sub>6</sub>DMSO.  
38

### 39 40 41 FTIR analysis

42  
43 The IR absorption bands for free p-anisic acid were observed at 3000-2545 cm<sup>-1</sup> (O-H  
44 stretching), 1786 cm<sup>-1</sup> (C=O stretch), 1603 cm<sup>-1</sup> and 1517 cm<sup>-1</sup> (C=C stretch) of the aromatic  
45 ring (**Figure 3a**). The FTIR spectra of DSPE-PEG-Amine shows characteristic peaks at 2919  
46 cm<sup>-1</sup> (C-H stretch), 1114 cm<sup>-1</sup> (C-O stretch), and the peaks at 1468 cm<sup>-1</sup>, 1345 cm<sup>-1</sup>, 952 cm<sup>-1</sup>  
47 and 842 cm<sup>-1</sup> also belong to the PEG (**Figure 3b**). The absorbance bands characteristic of  
48 amide coupling observed in the FT-IR spectrum of DSPE-PEG5000-Anisic acid were 1628  
49 cm<sup>-1</sup> (Amide I) and 1574 cm<sup>-1</sup> (Amide II) (**Figure 3c**). The relative intensities of these bands  
50  
51  
52  
53  
54  
55  
56  
57  
58  
59  
60



(1:0.3) is that expected for secondary acyclic amides. This confirmed coupling of p-anisic acid with DSPE-PEG-Amine

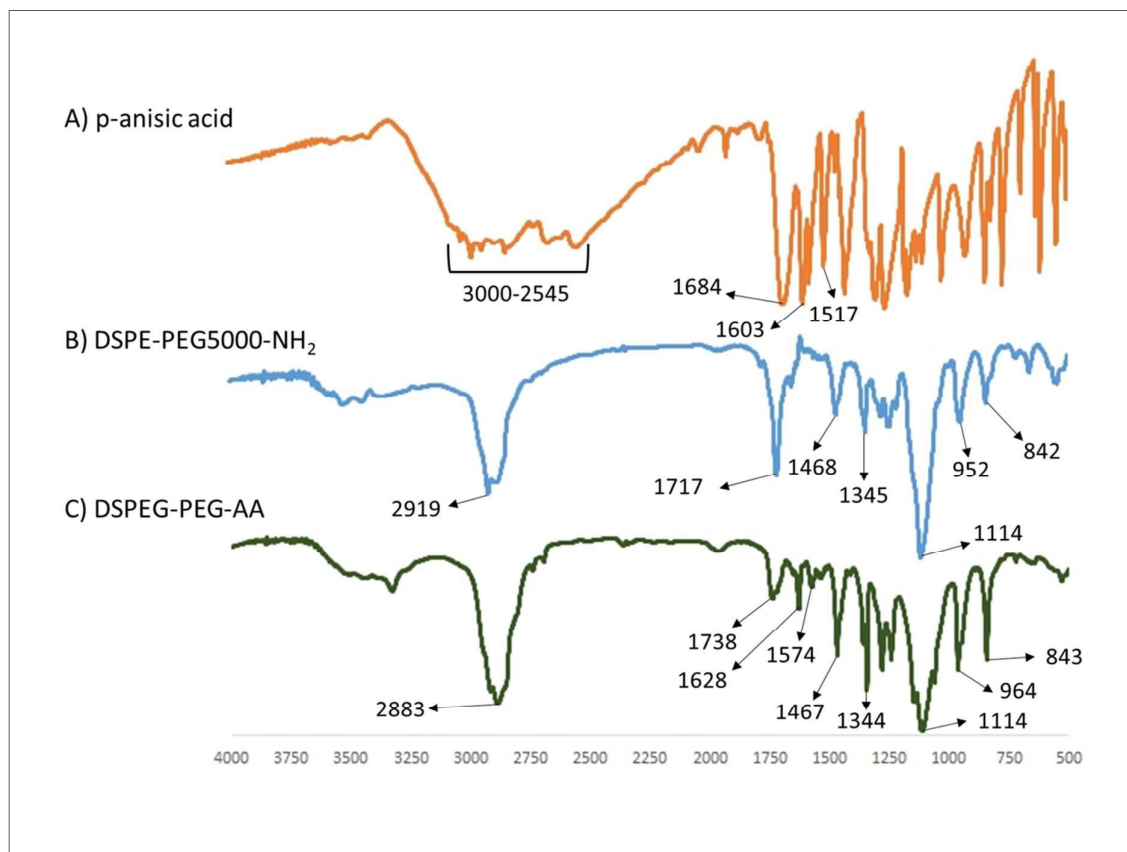


**Figure 3:** FTIR analysis of A) *p*-anisic acid, B) DSPE-PEG<sub>5000</sub>-NH<sub>2</sub> and C) DSPE-PEG<sub>5000</sub>-anisamide.

### Physicochemical characterisation of Cyclodextrin nanoparticles

DSPE-PEG<sub>5000</sub> was post inserted into pre-formed CD.siRNA nanoparticles. Interestingly, following the addition of DSPE-PEG<sub>5000</sub> the nanoparticles decreased in size (between 60-80 nm) as measured using Dynamic Light Scattering (DLS) (Table 1). It has previously been reported that the co-formulation of a cationic CD vector with a PEGylated CD likewise resulted in a smaller particle diameter<sup>30</sup>. Cationic NPs are generally more cytotoxic in nature than their neutral counterparts; this can be due to disruption of the plasma membrane as well

as significant mitochondrial and lysosomal damage<sup>31</sup>. The addition of PEG onto the surface of cationic NPs has been shown to reduce the surface charge as well as attenuate non-specific binding to serum proteins following systemic delivery<sup>32, 33</sup>. The addition of DSPE-PEG<sub>5000</sub> significantly ( $p < 0.001$ ) reduced the zeta potential of nanoparticles from  $+46.42 \pm 1.67$  mV to between  $+20.74$  and  $+23.40$  mV (**Table 1**). A significant reduction in the cationic surface charge of CD nanoparticles has previously been reported following insertion of DSPE-PEG<sub>5000</sub> into preformed CD.siRNA complexes<sup>34</sup>.

**Table 1:** Physicochemical properties of CD.siRNA complexes before and after the incorporation of DSPE-PEG<sub>5000</sub> by the post-insertion method. Data is presented as the mean  $\pm$  SD ( $n=5$ ).

Formulation	Formulation abbreviation	Molar Ratio of CD:DSPE-PEG <sub>5000</sub> -Anisamide:DSPE-PEG <sub>5000</sub> -Methyl:DSPE-PEG <sub>2000</sub> -R8		Diameter (nm)	PDI	Zeta Potential (mV)
UnPEGylated CD.siRNA	CCD	1:0:0		$202.90 \pm 20.41$	$0.33 \pm 0.04$	$46.42 \pm 1.67$
Targeted (PEGylated) CD.siRNA (R8 +)	TR8+	1 : 0.75 : 0 : 0.10		$132.42 \pm 7.97$	$0.29 \pm 0.03$	$23.40 \pm 1.50$
Targeted (PEGylated) CD.siRNA (R8 -)	TR8-	1 : 0.75 : 0 : 0		$137.04 \pm 6.72$	$0.31 \pm 0.04$	$20.74 \pm 2.27$
Untargeted (PEGylated) CD.siRNA (R8 +)	UR8+	1 : 0 : 0.75 : 0.10		$146.08 \pm 5.56$	$0.35 \pm 0.03$	$23.06 \pm 1.74$

1  
2  
3 An integral factor in the development of an effective non-viral gene delivery vector for *in*  
4 *vivo* applications is the ability of the vector to protect siRNA from serum nucleases which  
5 can potentially degrade siRNA. It has previously been shown that free siRNA can be  
6 degraded in as little as 1 min in the presence of physiological concentrations of serum <sup>34</sup>. In  
7 contrast, as demonstrated in this study, when siRNA is complexed with the untargeted but  
8 PEGylated CD.siRNA complex, siRNA degradation does not occur until approximately 8 h  
9 (UR8+). Furthermore, the addition of a targeting ligand (TR8+) led to no detectable  
10 degradation even at the 8 h time point (**Figure 4a**).  
11  
12  
13  
14  
15  
16  
17  
18  
19  
20  
21  
22  
23  
24  
25  
26  
27  
28  
29  
30  
31  
32  
33  
34  
35  
36  
37  
38  
39  
40  
41  
42  
43  
44  
45  
46  
47  
48  
49  
50  
51  
52  
53  
54  
55  
56  
57  
58  
59  
60

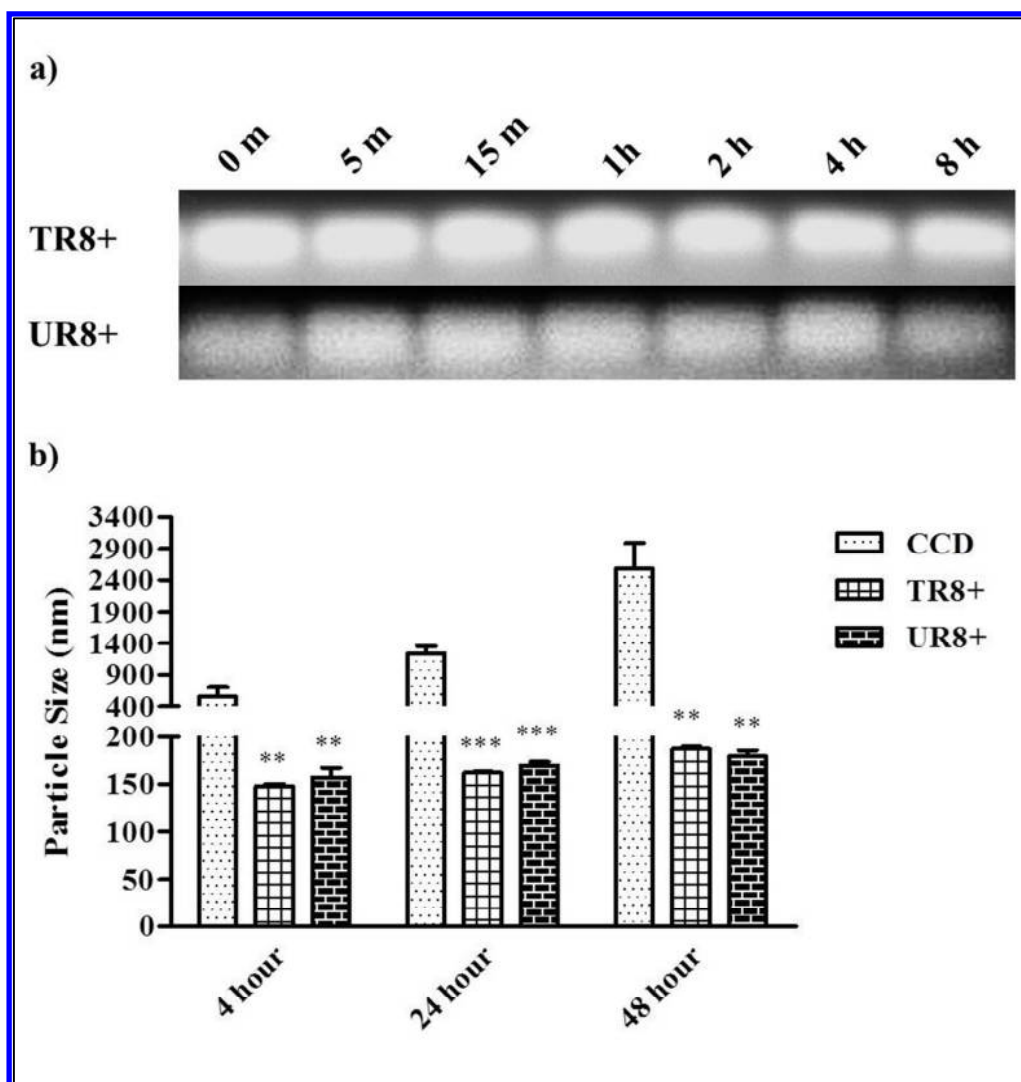


**Figure 4: Assessment of the modified CD.siRNA nanoparticles in physiological conditions.**

(a) Serum stability of targeted CD (TR8+) (top) and untargeted CD (UR8+) (bottom) in physiological concentrations of FBS over 8 h. (b) Aggregation of CD formulations in physiological salt concentrations over 4, 24 and 48 h (\*\* $p < 0.01$ ), (\*\*\*) $p < 0.001$ ). Data are presented as mean  $\pm$  SD ( $n=4$ ).

1  
2  
3 The ability of the modified CD to resist aggregation in physiological salt concentrations was  
4  
5 also investigated. As seen in **figure 4b**, the CCD complexes tended to aggregate, reaching  
6  
7 particle sizes of greater than 1000 nm after 24 h. In contrast, both of the R8-containing  
8  
9 PEGylated nanoparticles (TR8+ and UR8+) resisted aggregation up to 48 h and maintained  
10  
11 particle sizes of approximately 180-190 nm.  
12

### 13 14 15 **Toxicity and immunotoxicity of CD nanoparticles *in vitro*.**

16  
17  
18 The cyclodextrin-containing formulations under investigation in this study (CCD, UR8+,  
19  
20 TR8+ and TR8-) did not elicit a cytotoxic response in either PC3 or DU145 prostate cancer  
21  
22 cells when compared to untreated controls as measured using the MTT assay (**Figure 5**). The  
23  
24 cationic CD formulation (CCD) used in this study has previously been shown to be non-toxic  
25  
26 in a range of different cell lines including neuronal mouse mHypoE-N41 cells, human  
27  
28 prostate PC3 cells and human astrogloma U87 cells <sup>12, 13, 30</sup>. In contrast, the lipofectamine  
29  
30 control displayed significant levels of reduction in cell viability for both cell lines over the 48  
31  
32 h period (p<0.001).  
33  
34  
35  
36  
37  
38  
39  
40  
41  
42  
43  
44  
45  
46  
47  
48  
49  
50  
51  
52  
53  
54  
55  
56  
57  
58  
59  
60

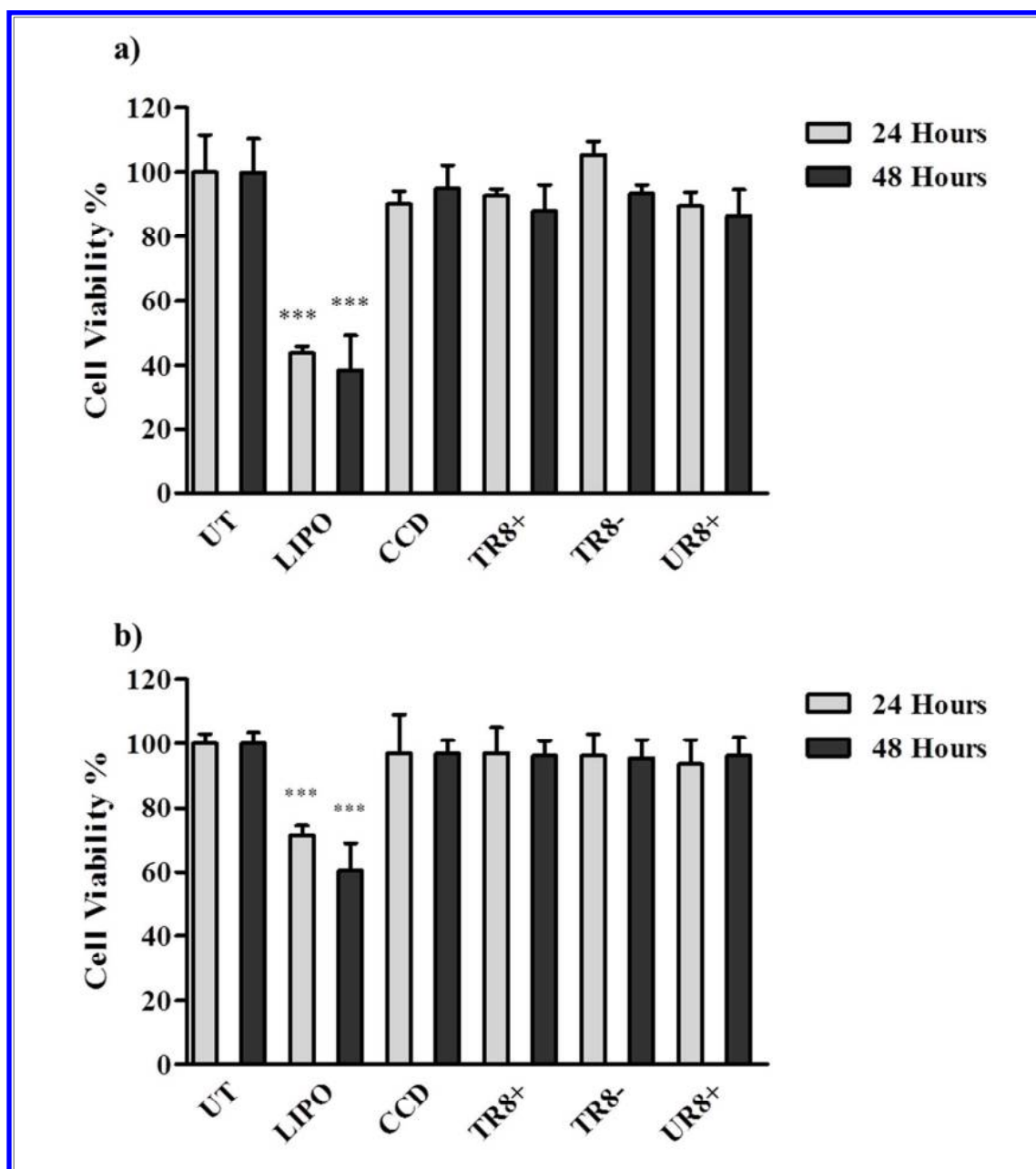


**Figure 5:** Cytotoxicity of CD complexes. Toxicity of the CD complexes was determined by MTT assay in PC3 (a) and DU145 (b) cells 24 and 48 h following transfection with 100 nM siRNA. Data are expressed as mean  $\pm$  SD ( $n=4$ ). (\*\*\*)  $p < 0.001$  relative to the untreated control).

1  
2  
3 In order to determine if the CD complexes under investigation elicited an immune response,  
4 the complexes were incubated with mouse macrophage RAW264.7 cells<sup>12</sup>. LPS was used as  
5 a positive control and changes in the levels of two inflammatory-related cytokines;  
6 cyclooxygenase-2 (COX-2) and tumour necrosis factor alpha (TNF- $\alpha$ ) were monitored.  
7  
8  
9

10  
11  
12 COX-2 is a cyclooxygenase that metabolises arachidonic acid to prostaglandins. It is a key  
13 regulator of inflammation and has been shown to be induced by exogenous stimuli<sup>35</sup>.  
14  
15 Previous studies have shown that several different types of nanoparticles, including multi-  
16 wall carbon nanotubes, silica, silver, aluminium and carbon black nanoparticles, induce an  
17 increase in the expression of COX-2 in macrophages<sup>36-39</sup>. For each of the CD-containing  
18 formulations tested, only a modest increase in COX-2 mRNA levels (1.4 to 5.4-fold) was  
19 observed (**Figure 6a**). However, this increase was not statistically significant from the  
20 untreated control. In contrast, the use of LPS showed a significant increase ( $p < 0.001$ ) in  
21 COX-2 mRNA levels of approximately 300 and 2000 fold after 4 and 24 h respectively.  
22  
23  
24  
25  
26  
27  
28  
29  
30  
31  
32

33 TNF- $\alpha$  is a key pro-inflammatory cytokine involved in the innate immune response<sup>40</sup>.  
34  
35 Interestingly, it is cytotoxic to tumour cells under certain conditions, however, due to its pro-  
36 inflammatory nature it can also promote tumour angiogenesis and tumour growth<sup>41, 42</sup>.  
37  
38 DOTAP and multi-walled carbon nanotubes complexed with siRNA have been shown to  
39 significantly induce TNF- $\alpha$  expression<sup>43, 44</sup>. As with COX-2, the modest increases (between  
40 1.2 to 2.7- fold) in TNF- $\alpha$  induction following incubation with any of the CD formulations  
41 were not significant relative to the untreated control (**Figure 6b**) ( $p > 0.05$ ). The LPS positive  
42 control significantly increased TNF- $\alpha$  expression ( $p < 0.001$ ) by approximately 14.4 and 24-  
43 fold increase after 4 and 24 h, respectively.  
44  
45  
46  
47  
48  
49  
50  
51  
52  
53

54 These results support a previous study, published by our group, where the amphiphilic  
55 cationic CD formulations failed to induce COX-2 and TNF- $\alpha$  expression in a BV2 microglial  
56  
57  
58  
59  
60

1  
2  
3 cell line <sup>12</sup>. The above data demonstrate that the CD nanoparticles do not induce either a  
4  
5 cytotoxic or immunotoxic profile in the cell lines tested.  
6  
7  
8  
9  
10  
11  
12  
13  
14  
15  
16  
17  
18  
19  
20  
21  
22  
23  
24  
25  
26  
27  
28  
29  
30  
31  
32  
33  
34  
35  
36  
37  
38  
39  
40  
41  
42  
43  
44  
45  
46  
47  
48  
49  
50  
51  
52  
53  
54  
55  
56  
57  
58  
59  
60



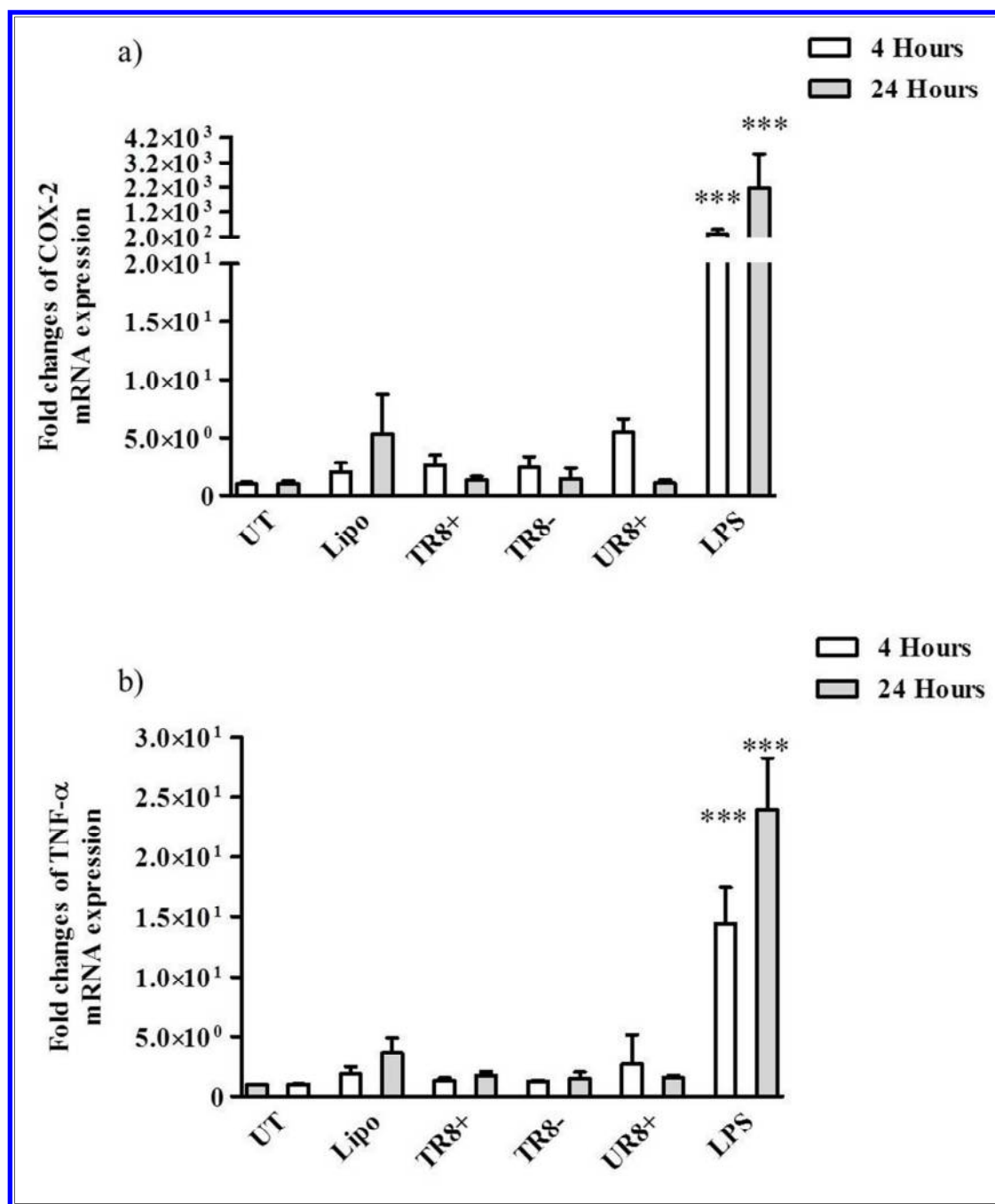


**Figure 6:** Fold changes in the expression of mRNA for pro inflammatory cytokines (COX-2 (a) and TNF- $\alpha$  (b)) in RAW246.7 cells following incubation with CD.siRNA complexes for 4 h (white) and 24 h (grey). LPS (10 ng/ml) was used as a positive control. Data are represented as mean  $\pm$  SD (n=3) (\*\*\*)  $p < 0.001$  relative to the untreated control).

### Competitive inhibition assay

Cellular uptake of the CD formulations was investigated in two sigma receptor positive cell lines; PC3 and DU145 cells. The TR8+ nanoparticles showed significantly higher uptake in PC3 cells compared to UR8+ (**Figure 7a**) ( $p < 0.05$ ) in accordance with previous studies which showed increased uptake of anisamide targeted nanoparticles in sigma receptor positive cells relative to untargeted nanoparticles<sup>15, 45</sup>. For the DU145 cell line (**Figure 7b**), while there was a greater uptake for the TR8+ formulation when compared with UR8+, this difference did not reach statistical significance ( $p > 0.05$ ). While there is evidence of the specific uptake of targeted nanoparticles in PC3 and DU145 cells, there does appear to be a relevant amount of uptake that is receptor-independent or non-specific. Many different physicochemical properties of nanoparticles contribute to their cellular uptake, with one of the contributors being the surface charge<sup>46</sup>. Positively charged nanoparticles increase their non-specified affinity to the negatively charged plasma membrane and their subsequent uptake into cells<sup>47</sup>. While there was an observed reduction in the surface charge of the cyclodextrin nanoparticles following the inclusion of PEG into the formulation (from 46 mV to ~25 mV) (**Table 1**), these nanoparticles are still cationic in nature. It is hypothesised that this cationic nature is contributing to the non-specific uptake observed in **figure 7**.

Haloperidol has a high affinity for the sigma receptor and has previously been used in competition assays to demonstrate sigma receptor-mediated uptake of anisamide-linked nanoparticles<sup>14, 15</sup>. In the current study, a significant reduction ( $p < 0.05$ ) in the uptake of TR8+ nanoparticles in both PC3 and DU145 cells following 4 h pre-incubation with 40  $\mu\text{M}$  haloperidol was observed (**Figure 7a and 7b** respectively). In contrast, no reduction in the uptake of UR8+ nanoparticles following haloperidol pre-incubation occurred. These results support the evidence for sigma-receptor mediated uptake of anisamide-targeted nanoparticles in PC3 and DU145 cells. In anticipation of R8 interfering with the targeting ability of

1  
2  
3 anisamide on the surface of the nanoparticle, a shorter PEG length of PEG<sub>2000</sub> was adopted  
4  
5 for R8 relative to the anisamide ligand (PEG<sub>5000</sub>). A similar strategy was recently used by  
6  
7 *Xiang et al.* where a CPP was attached to a PEG chain with a lower molecular weight relative  
8  
9 to that containing a folate targeting ligand <sup>32</sup>. The fact that the targeted formulation showed a  
10  
11 significant reduction in uptake following pre-incubation with haloperidol in both cell lines  
12  
13 highlights that the incorporation of DSPE-PEG<sub>2000</sub>-R8 did not interfere with the targeting  
14  
15 ability of anisamide on the surface of the nanoparticles.  
16  
17

18  
19 There is some controversy relating to the targeting specificity of anisamide to either the  
20  
21 sigma 1 receptor (S1-R) or the sigma 2 receptor (S2-R) <sup>48</sup>. Depending on the cell line in  
22  
23 question, the localisation of S1-R can either be intracellular or alternatively on the cell  
24  
25 surface <sup>49, 50</sup>. It is still unknown whether anisamide preferentially binds S1-R or S2-R and  
26  
27 further work to determine S1-R localisation in prostate cancer cell lines is currently ongoing.  
28  
29  
30  
31  
32  
33  
34  
35  
36  
37  
38  
39  
40  
41  
42  
43  
44  
45  
46  
47  
48  
49  
50  
51  
52  
53  
54  
55  
56  
57  
58  
59  
60

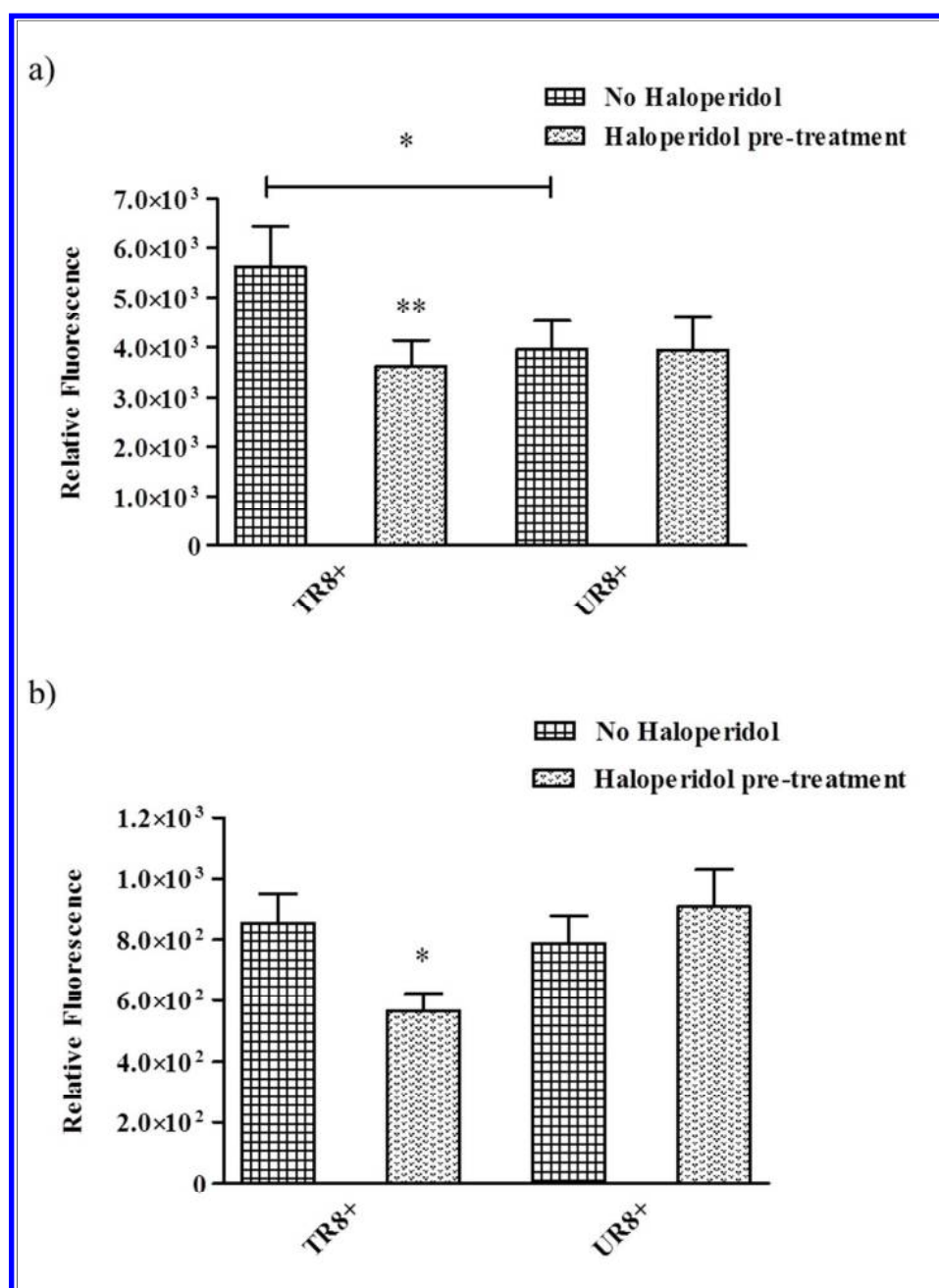


**Figure 7:** Uptake of 6-FAM labelled siRNA (50 nM) complexed with TR8+ and UR8+ into (a) PC3 and (b) DU145 cells. For haloperidol pre-treatment, cells were treated with 40  $\mu$ M haloperidol for 4 h prior to transfection. 4 h after transfection, cells were lysed and uptake was analysed by quantification of the fluorescent intensity normalised to protein content. Data are presented as mean  $\pm$  SD (n=3) (\* $p$ <0.05, \*\* $p$ <0.01).

## Knockdown of polo-like kinase 1 (PLK1) in 2D

Polo-like kinase 1 (PLK1) is a key regulator of the cell cycle. It is known to be overexpressed in prostate cancer cells, with a high level of PLK1 expression correlating to poor patient outcomes<sup>51</sup>. The use of ATP-competitive inhibitors of PLK1 *in vivo* has been reported to be of therapeutic value in various cancers<sup>52, 53</sup>. Several studies have also shown efficacy in treating various cancers by silencing PLK1 using siRNA<sup>54-56</sup>. In a recent study, PLK1 siRNA was encapsulated in a PSMA-targeted liposomal formulation and produced a significant increase in the levels of apoptosis in the prostate cancer cell line, 22RV1 cells. In a 22RV1 xenograft model, liposomes containing PLK1 siRNA showed a significant reduction in tumour volume compared to an untreated control<sup>32</sup>. Due to the previous successes of PLK1 siRNA in the treatment of prostate cancer, it was chosen for the present study.

The ability of the targeted formulations to silence PLK1 was initially evaluated in 2D prostate cancer cell culture. In 2D *in vitro* silencing studies (**Figure 8**), while the level of PLK1 mRNA knockdown tended to be greater with the targeted (TR8+) versus the untargeted (UR8+) formulation, the differences were not significantly different in either cell line (PC3 cells: ~ 40 % knockdown for both TR8+ and UR8+ (**Figure 8a**), DU145 cells: 55 % knockdown for TR8+, ~ 40 % for UR8+ (**Figure 8b**)). These levels of gene silencing were superior to those reported previously for anisamide targeted hydrophilic CD nanoparticles<sup>16</sup>. In the absence of R8, there was no significant PLK1 gene knockdown compared to the non-silencing control in either cell line. The positive effect of R8 reported in this study is consistent with previous results where the incorporation of R8 into a CD formulation resulted in enhanced gene knockdown in a neuronal cell line<sup>18</sup>.

1  
2  
3 A similar trend was observed in the levels of luciferase reporter gene knockdown when  
4  
5 luciferase siRNA was incorporated into targeted (TR8- and TR8+) and untargeted  
6  
7 nanoparticles (UR8+) (**Supplementary Figure 1**).  
8  
9  
10  
11  
12  
13  
14  
15  
16  
17  
18  
19  
20  
21  
22  
23  
24  
25  
26  
27  
28  
29  
30  
31  
32  
33  
34  
35  
36  
37  
38  
39  
40  
41  
42  
43  
44  
45  
46  
47  
48  
49  
50  
51  
52  
53  
54  
55  
56  
57  
58  
59  
60

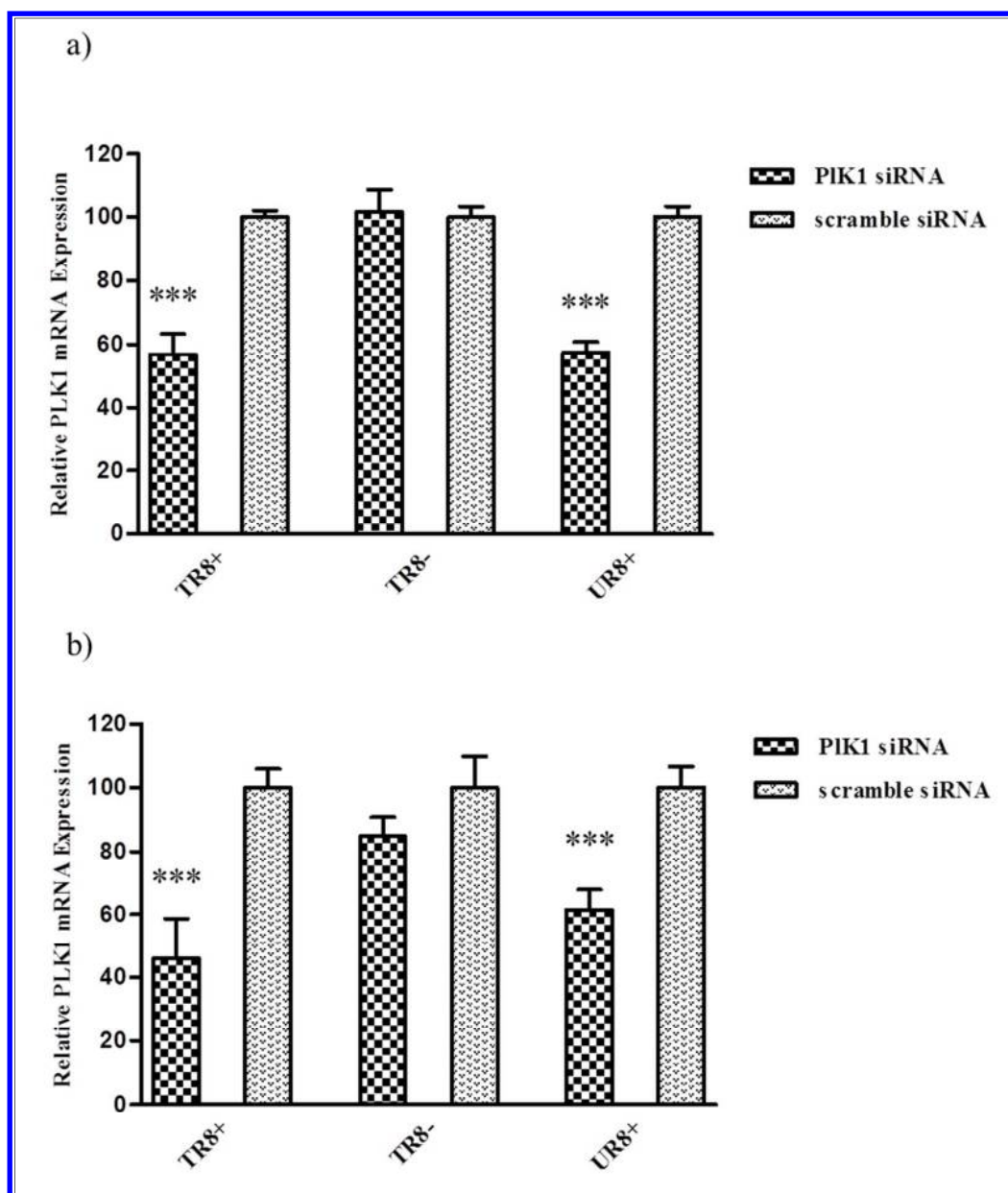


**Figure 8:** Knockdown of PLK1 gene in PC3 (a) and DU145 cells (b) using 100 nM siRNA.

PLK1 gene expression was normalised to the non-silencing counterpart whose expression was set to 100 %. Data are presented as mean  $\pm$  SD ( $n=3$ ) ( $p^{***}<0.001$ ).

### Uptake and knockdown of PLK1 in cells grown in 3D.

The vast majority of cancer studies *in vitro* are conducted using two-dimensional (2D) techniques involving petri dishes and plastic wells<sup>57</sup>. These conventional 2D methods often

1  
2  
3 fail to mimic the complex microenvironment that is present in cancerous tissues <sup>58</sup>. For  
4  
5 example, it was recently shown that when LNCaP cells were grown in a 3D environment,  
6  
7 they were more resistant to docetaxel treatment than when grown in 2D <sup>22, 59</sup>. Such studies  
8  
9 highlight the need to move away from 2D cell-culture models to more clinically relevant 3D  
10  
11 study models in order to more accurately determine the cellular response to drugs under  
12  
13 development <sup>25</sup>. Although 3D models are to date not routinely used for drug assessment  
14  
15 during *in vitro* development, a wide range of options for culturing cells in 3D are now  
16  
17 available including spheroids, scaffolds, organotypes and explants <sup>60</sup>.

20  
21 A recent study described the use of collagen-nanohydroxyapatite-based scaffolds (containing  
22  
23 5-fold nanohydroxyapatite relative to collagen (i.e.S500)) to simulate a physiologically  
24  
25 relevant 3D prostate cancer metastases model <sup>22</sup>. These scaffolds have been engineered to  
26  
27 have a porous structure that allows for the infiltration of both cells and nutrients <sup>27</sup>. In the  
28  
29 study, two prostate cancer cell lines (LNCaP and PC3 cells) were shown to infiltrate and  
30  
31 proliferate on the scaffolds, but at a slower rate when compared to 2D counterparts <sup>22</sup>. Cells  
32  
33 also demonstrated increased resistance to docetaxel treatment when cultured on this specific  
34  
35 collagen-based scaffold suggesting enhanced physiological relevance relative to standard 2D  
36  
37 cell culture on plastic tissue culture plates. Thus, in the present study, we have used this 3D  
38  
39 model for the first time to investigate the ability of the targeted nanoparticles (TR8+) to  
40  
41 deliver siRNA to sigma receptor positive prostate cancer cells in an *in vitro* bone metastatic  
42  
43 model.  
44  
45  
46  
47

48  
49 **Figure 9** shows the uptake of 6-FAM-labelled siRNA (either alone, or complexed in a  
50  
51 targeted CD nanoparticle) at 24 and 48 h in either PC3 (left) or DU145 (right) cells grown on  
52  
53 S500 scaffolds. In the case of the TR8+ nanoparticle, it is clear that fluorescent siRNA is  
54  
55 present within the boundary of the cell membrane for both cell lines at 24 and 48 h. In  
56  
57 contrast, for the naked siRNA, no siRNA was visible within the cell membrane at either of  
58  
59  
60



1  
2  
3 the time points. These results indicate that the targeted CD nanoparticles can effectively  
4  
5 deliver siRNA to prostate cancer cells that have been cultured in 3D on a S500 scaffold.  
6  
7  
8  
9  
10  
11  
12  
13  
14  
15  
16  
17  
18  
19  
20  
21  
22  
23  
24  
25  
26  
27  
28  
29  
30  
31  
32  
33  
34  
35  
36  
37  
38  
39  
40  
41  
42  
43  
44  
45  
46  
47  
48  
49  
50  
51  
52  
53  
54  
55  
56  
57  
58  
59  
60

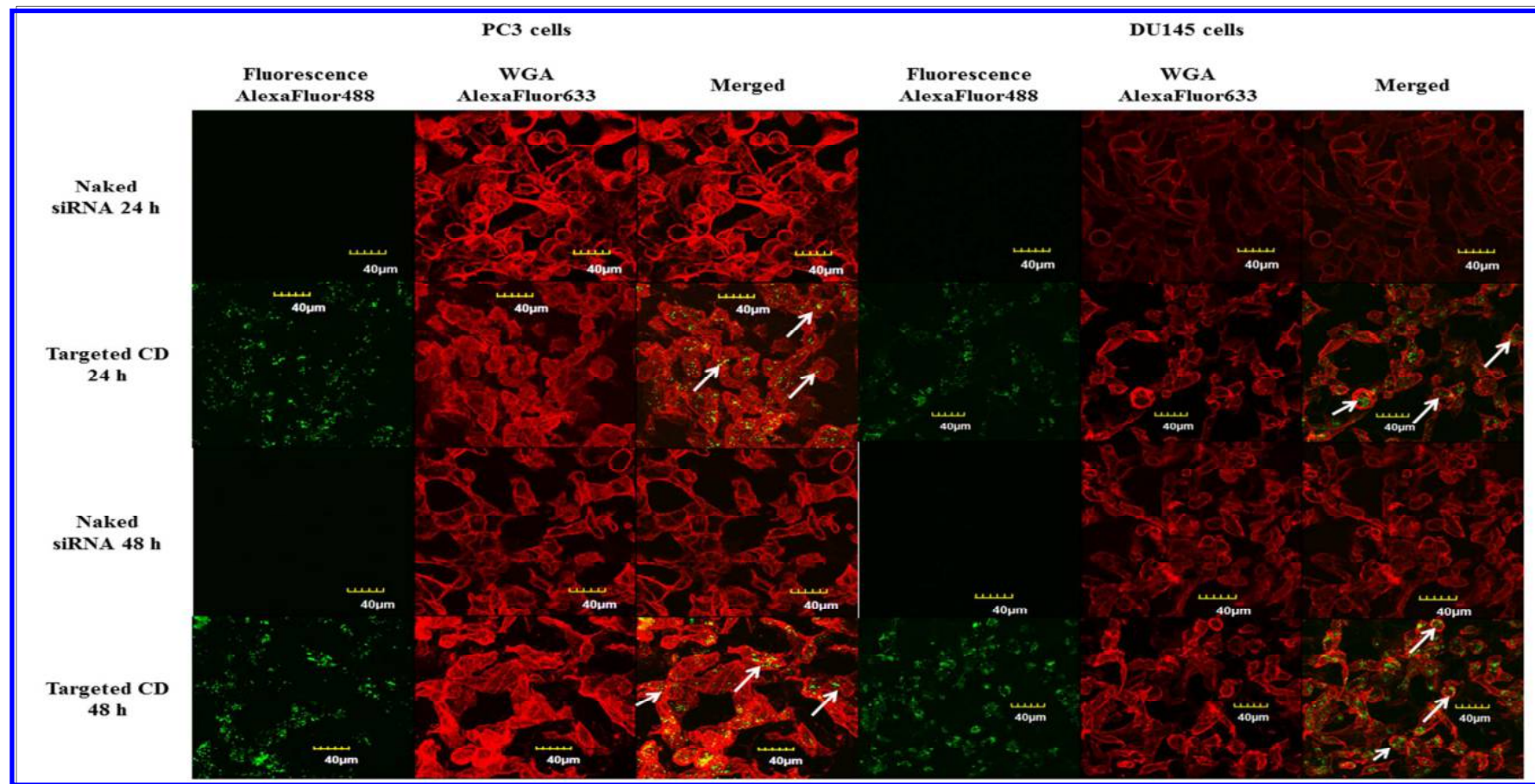
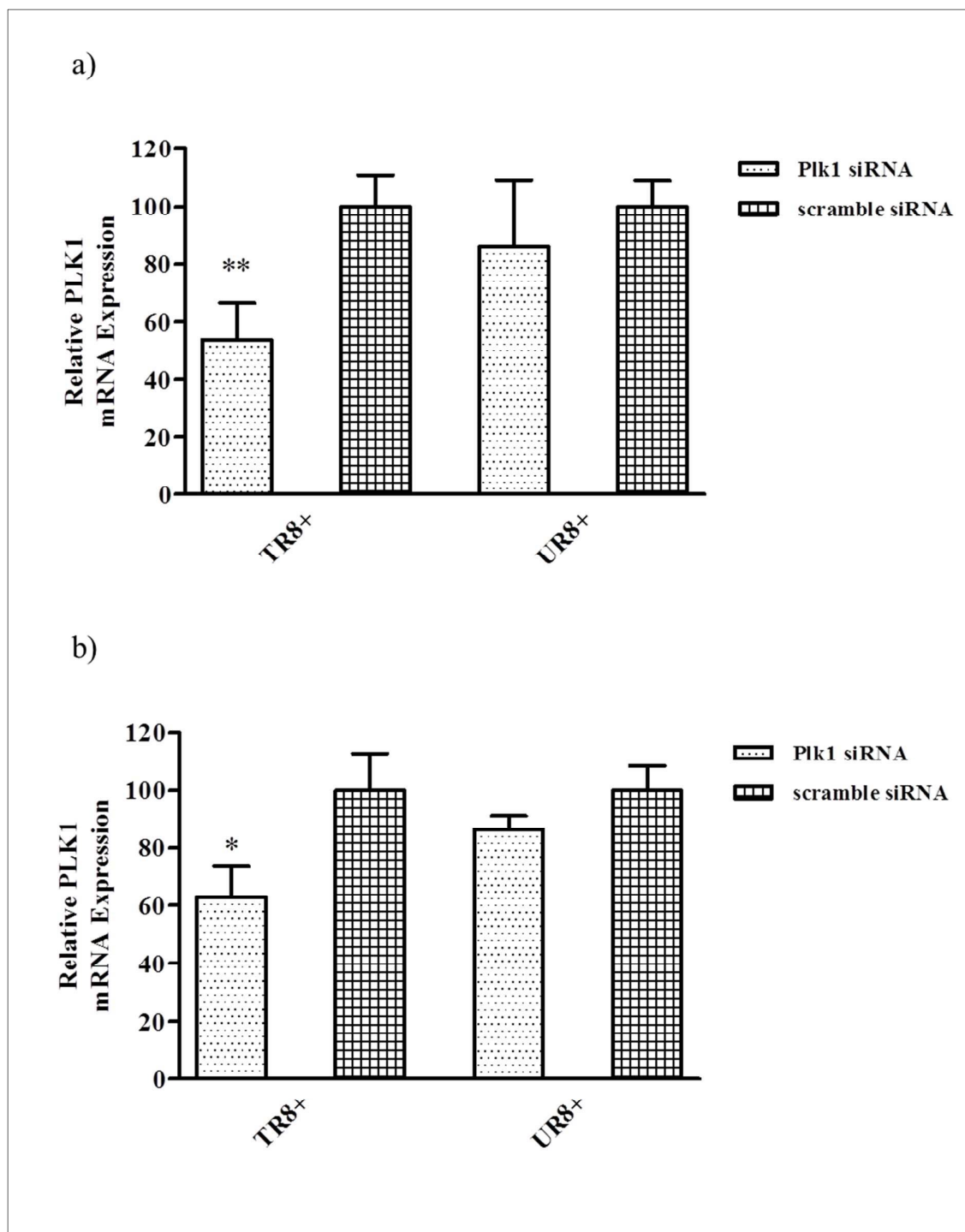


**Figure 9:** Uptake of fluorescent siRNA into PC3 (left) and DU145 (right) cells grown on S500 scaffolds either complexed in targeted CD or as naked siRNA for 24 or 48 h. Cell membrane was labelled with Alexa 633 (red) and the siRNA was labelled with 6-FAM (shown in green). siRNA within the cell boundary is marked with white arrows.



53 **Figure 10:** Knockdown of PLK1 in a) PC3 and b) DU145 cells grown on S500 scaffolds 48 h  
54 following transfection. PLK1 gene expression was normalised to the non-silencing  
55 counterpart whose expression was set to 100 %. Data are presented as mean  $\pm$  SD (n=4).  
56  
57  
58  
59  
60

1  
2  
3 When the cells on the scaffold were transfected with the targeted nanoparticles, significant  
4 reductions in the levels of PLK1 mRNA (approximately 45 % and 40 % for PC3 and DU145,  
5 respectively) were observed compared to the non-silencing controls. In contrast, the levels of  
6 gene silencing (approximately 15 %) observed in both cell lines with the untargeted  
7 formulations were not statistically significant versus the control.  
8  
9

10  
11  
12  
13  
14  
15 In 3D, the levels of PLK1 mRNA knockdown mediated by the targeted nanoparticles were  
16 significantly greater than the untargeted nanoparticles in both PC3 ( $p=0.0425$ ) and DU145  
17 cells ( $p=0.0269$ ). The differences in the levels of PLK1 mRNA knockdown between cells  
18 grown in 2D versus 3D are summarised in **table 2**. The advantages of the targeted delivery  
19 system appear to be masked in the 2D culture (**Figure 10**), as similar levels of knockdown  
20 are seen for both the targeted and untargeted formulations. In contrast, the incorporation of  
21 the anisamide-targeting ligand into the formulation shows a greater level of knockdown  
22 versus the untargeted formulation in the 3D scaffold model (**Figure 10**). Previous studies  
23 have highlighted similar discrepancies when delivering genetic material to cells grown in 2D  
24 versus 3D. In a recent study, 3D porous chitosan-alginate scaffolds were used to grow  
25 TRAMP-C2 prostate cancer cells. Targeted iron oxide NPs and untargeted NPs were used to  
26 deliver a gene for red fluorescent protein (RFP); in 2D no differences between the targeted  
27 and untargeted formulations, with regards to both uptake and transfection, were observed. In  
28 contrast, when cells were grown in 3D, there was an approximate 2-fold increase in RFP  
29 expression for the targeted formulations, with no difference observed for the untargeted  
30 formulation. In addition, due to the enhanced malignant microenvironment in the 3D model it  
31 was hypothesized that the expression level of the target receptor, MMP-2, was increased, thus  
32 providing a greater number of cell surface receptors for attachment of the targeted NP <sup>61</sup>.  
33  
34  
35  
36  
37  
38  
39  
40  
41  
42  
43  
44  
45  
46  
47  
48  
49  
50  
51  
52  
53

54  
55  
56 **Table 2:** Summary of the level of knockdown of PLK1 in PC3 and DU145 cells grown in 2D  
57 and 3D ( $*p<0.05$ ,  $n=3$ ).  
58  
59  
60

<b>Cell Line</b>	<b>Sample</b>	<b>2D</b>	<b>3D</b>
<b>PC3</b>	<b>TR8+</b>	43.09 ± 1.39	46.09 ± 12.54
	<b>UR8+</b>	42.58 ± 1.18	13.93 ± 23.21
	<b>Significance</b>	p=0.8567	p=0.0425(*)
<b>DU145</b>	<b>TR8+</b>	54.01 ± 12.66	37.27 ± 11.06
	<b>UR8+</b>	38.59 ± 6.41	13.50 ± 4.81
	<b>Significance</b>	p=0.115	P=0.0269(*)

## Conclusions

Treating advanced prostate cancer is a challenge for clinicians with current therapies offering only a modest survival benefit. RNAi has significant potential for treating disease, with the development of an effective delivery vector being the main barrier to clinical translation. In this study, a CD-based anisamide targeted nanoparticle was formulated to exploit specific uptake via the sigma receptor, known to be overexpressed in prostate cancer cells. When assessed in a 2D cell model, while the targeted formulation resulted in slightly greater levels of gene knockdown, the untargeted formulation produced a high degree of non-specific uptake which also translated into significant gene silencing. In contrast, in the 3D model, significant gene silencing was detected only with the targeted formulation implying that this model was more effective at distinguishing between targeted and untargeted formulations. This apparent superior performance of the 3D model may be related to a higher level of sigma receptor expression by cells in a 3D environment, as suggested previously in the case of the MMP-2 receptor (52). In addition, the geometry of the scaffold may facilitate a more favourable presentation or orientation of the receptor thus promoting specific receptor-ligand binding.

It is hoped that this 3D *in vitro* model of bone cancer metastasis will provide a biopharmaceutically relevant tool to more accurately predict the *in vivo* response to RNAi therapeutics thus reducing the need for pre-clinical animal studies. To our knowledge, this is the first example of the use of a targeted CD nanoparticle to deliver siRNA to prostate cancer cells grown in a 3D model of bone metastasis.

## References

1. Haas, G. P.; Delongchamps, N.; Brawley, O. W.; Wang, C. Y.; de la Roza, G. The worldwide epidemiology of prostate cancer: perspectives from autopsy studies. *The Canadian journal of urology* **2008**, *15*, (1), 3866.
2. Siegel, R. L.; Miller, K. D.; Jemal, A. Cancer statistics, 2015. *CA: a cancer journal for clinicians* **2015**, *65*, (1), 5-29.
3. Mohan, R.; Schellhammer, P. F. Treatment options for localized prostate cancer. *Am Fam Physician* **2011**, *84*, (4), 413-20.
4. Yin, L.; Hu, Q.; Hartmann, R. W. Recent progress in pharmaceutical therapies for castration-resistant prostate cancer. *Int J Mol Sci* **2013**, *14*, (7), 13958-78.
5. Shafi, A. A.; Yen, A. E.; Weigel, N. L. Androgen receptors in hormone-dependent and castration-resistant prostate cancer. *Pharmacology & therapeutics* **2013**, *140*, (3), 223-238.
6. Almeida, R.; Allshire, R. C. RNA silencing and genome regulation. *Trends in cell biology* **2005**, *15*, (5), 251-258.
7. Aagaard, L.; Rossi, J. J. RNAi therapeutics: principles, prospects and challenges. *Advanced drug delivery reviews* **2007**, *59*, (2), 75-86.
8. Guo, J.; Evans, J. C.; O'Driscoll, C. M. Delivering RNAi therapeutics with non-viral technology: a promising strategy for prostate cancer? *Trends Mol Med* **2013**, *19*, (4), 250-61.
9. Mellet, C. O.; Fernández, J. M. G.; Benito, J. M. Cyclodextrin-based gene delivery systems. *Chemical Society Reviews* **2011**, *40*, (3), 1586-1608.
10. McCarthy, J.; O'Neill, M. J.; Bourre, L.; Walsh, D.; Quinlan, A.; Hurley, G.; Ogier, J.; Shanahan, F.; Melgar, S.; Darcy, R.; O'Driscoll, C. M. Gene silencing of TNF-alpha in a murine model of acute colitis using a modified cyclodextrin delivery system. *Journal of Controlled Release* **2013**, *168*, (1), 28-34.
11. McMahan, A.; O'Neill, M. J.; Gomez, E.; Donohue, R.; Forde, D.; Darcy, R.; O'Driscoll, C. M. Targeted gene delivery to hepatocytes with galactosylated amphiphilic cyclodextrins. *Journal of Pharmacy and Pharmacology* **2012**, *64*, (8), 1063-1073.
12. Godinho, B. M. D. C.; McCarthy, D. J.; Torres-Fuentes, C.; Beltrán, C. J.; McCarthy, J.; Quinlan, A.; Ogier, J. R.; Darcy, R.; O'Driscoll, C. M.; Cryan, J. F. Differential nanotoxicological and neuroinflammatory liabilities of non-viral vectors for RNA interference in the central nervous system. *Biomaterials* **2014**, *35*, (1), 489-499.
13. Evans, J. C.; McCarthy, J.; Torres-Fuentes, C.; Cryan, J. F.; Ogier, J.; Darcy, R.; Watson, R. W.; O'Driscoll, C. M. Cyclodextrin mediated delivery of NF-kappaB and SRF siRNA reduces the invasion potential of prostate cancer cells in vitro. *Gene Ther* **2015**, *22*, (10), 802-10.
14. Banerjee, R.; Tyagi, P.; Li, S.; Huang, L. Anisamide-targeted stealth liposomes: A potent carrier for targeting doxorubicin to human prostate cancer cells. *International journal of cancer* **2004**, *112*, (4), 693-700.
15. Guo, J.; Ogier, J. R.; Desgranges, S.; Darcy, R.; O'Driscoll, C. Anisamide-targeted cyclodextrin nanoparticles for siRNA delivery to prostate tumours in mice. *Biomaterials* **2012**, *33*, (31), 7775-84.
16. Fitzgerald, K. A.; Malhotra, M.; Gooding, M.; Sallas, F.; Evans, J. C.; Darcy, R.; O'Driscoll, C. M. A novel, anisamide-targeted cyclodextrin nanoformulation for siRNA delivery to prostate cancer cells expressing the sigma-1 receptor. *International journal of pharmaceuticals* **2016**, *499*, (1), 131-145.
17. Johnson, R. M.; Harrison, S. D.; Maclean, D. Therapeutic applications of cell-penetrating peptides. *Cell-Penetrating Peptides: Methods and Protocols* **2011**, 535-551.
18. O'Mahony, A. M.; Desgranges, S.; Ogier, J.; Quinlan, A.; Devocelle, M.; Darcy, R.; Cryan, J. F.; O'Driscoll, C. M. In vitro investigations of the efficacy of cyclodextrin-siRNA complexes modified with lipid-PEG-Octaarginine: towards a formulation strategy for non-viral neuronal siRNA delivery. *Pharm Res* **2013**, *30*, (4), 1086-98.
19. Elliott, N. T.; Yuan, F. A review of three-dimensional in vitro tissue models for drug discovery and transport studies. *Journal of pharmaceutical sciences* **2011**, *100*, (1), 59-74.

- 1  
2  
3 20. Ravi, M.; Paramesh, V.; Kaviya, S.; Anuradha, E.; Solomon, F. 3D cell culture systems:  
4 advantages and applications. *Journal of cellular physiology* **2015**, *230*, (1), 16-26.
- 5 21. Knight, E.; Przyborski, S. Advances in 3D cell culture technologies enabling tissue-like  
6 structures to be created in vitro. *Journal of anatomy* **2015**, *227*, (6), 746-756.
- 7 22. Fitzgerald, K. A.; Guo, J.; Tierney, E. G.; Curtin, C. M.; Malhotra, M.; Darcy, R.; O'Brien, F. J.;  
8 O'Driscoll, C. M. The use of collagen-based scaffolds to simulate prostate cancer bone metastases  
9 with potential for evaluating delivery of nanoparticulate gene therapeutics. *Biomaterials* **2015**, *66*,  
10 53-66.
- 11 23. Lee, R. J.; Saylor, P. J.; Smith, M. R. Treatment and prevention of bone complications from  
12 prostate cancer. *Bone* **2011**, *48*, (1), 88-95.
- 13 24. Coleman, R. E. Clinical features of metastatic bone disease and risk of skeletal morbidity.  
14 *Clinical Cancer Research* **2006**, *12*, (20), 6243s-6249s.
- 15 25. Fitzgerald, K. A.; Malhotra, M.; Curtin, C. M.; O'Brien, F. J.; O'Driscoll, C. M. Life in 3D is  
16 never flat: 3D models to optimise drug delivery. *Journal of Controlled Release* **2015**, *215*, 39-54.
- 17 26. O'Mahony, A. M.; Godinho, B. M. D. C.; Ogier, J.; Devocelle, M.; Darcy, R.; Cryan, J. F.;  
18 O'Driscoll, C. M. Click-Modified Cyclodextrins as Nonviral Vectors for Neuronal siRNA Delivery. *ACS*  
19 *Chemical Neuroscience* **2012**, *3*, (10), 744-752.
- 20 27. Cunniffe, G. M.; Dickson, G. R.; Partap, S.; Stanton, K. T.; O'Brien, F. J. Development and  
21 characterisation of a collagen nano-hydroxyapatite composite scaffold for bone tissue engineering.  
22 *Journal of Materials Science: Materials in Medicine* **2010**, *21*, (8), 2293-2298.
- 23 28. Vader, P.; van der Aa, L. J.; Engbersen, J. F.; Storm, G.; Schiffelers, R. M. A method for  
24 quantifying cellular uptake of fluorescently labeled siRNA. *Journal of Controlled Release* **2010**, *148*,  
25 (1), 106-109.
- 26 29. El-Sayed, A.; Khalil, I. A.; Kogure, K.; Futaki, S.; Harashima, H. Octaarginine-and octalysine-  
27 modified nanoparticles have different modes of endosomal escape. *Journal of Biological Chemistry*  
28 **2008**, *283*, (34), 23450-23461.
- 29 30. O'Mahony, A. M.; Ogier, J.; Darcy, R.; Cryan, J. F.; O'Driscoll, C. M. Cationic and PEGylated  
30 amphiphilic cyclodextrins: co-formulation opportunities for neuronal siRNA delivery. *PLoS one* **2013**,  
31 *8*, (6), e66413.
- 32 31. Fröhlich, E. The role of surface charge in cellular uptake and cytotoxicity of medical  
33 nanoparticles. *Int J Nanomedicine* **2012**, *7*, 5577-5591.
- 34 32. Xiang, B.; Dong, D.-W.; Shi, N.-Q.; Gao, W.; Yang, Z.-Z.; Cui, Y.; Cao, D.-Y.; Qi, X.-R. PSA-  
35 responsive and PSMA-mediated multifunctional liposomes for targeted therapy of prostate cancer.  
36 *Biomaterials* **2013**, *34*, (28), 6976-6991.
- 37 33. Price, M.; Cornelius, R.; Brash, J. Protein adsorption to polyethylene glycol modified  
38 liposomes from fibrinogen solution and from plasma. *Biochimica et Biophysica Acta (BBA)-*  
39 *Biomembranes* **2001**, *1512*, (2), 191-205.
- 40 34. Evans, J. C.; Malhotra, M.; Guo, J.; O'Shea, J. P.; Hanrahan, K.; O'Neill, A.; Landry, W. D.;  
41 Griffin, B. T.; Darcy, R.; Watson, R. W.; O'Driscoll, C. M. Folate-targeted amphiphilic  
42 cyclodextrin.siRNA nanoparticles for prostate cancer therapy exhibit PSMA mediated uptake,  
43 therapeutic gene silencing in vitro and prolonged circulation in vivo. *Nanomedicine:*  
44 *Nanotechnology, Biology and Medicine* **2016**, *12*, (8), 2341-2351.
- 45 35. Shao, N.; Feng, N.; Wang, Y.; Mi, Y.; Li, T.; Hua, L. Systematic review and meta-analysis of  
46 COX-2 expression and polymorphisms in prostate cancer. *Molecular biology reports* **2012**, *39*, (12),  
47 10997-11004.
- 48 36. Lee, J. K.; Sayers, B. C.; Chun, K.-S.; Lao, H.-C.; Shipley-Phillips, J. K.; Bonner, J. C.;  
49 Langenbach, R. Multi-walled carbon nanotubes induce COX-2 and iNOS expression via MAP kinase-  
50 dependent and-independent mechanisms in mouse RAW264. 7 macrophages. *Particle and fibre*  
51 *toxicology* **2012**, *9*, (1), 1.
- 52 37. Park, E.-J.; Park, K. Oxidative stress and pro-inflammatory responses induced by silica  
53 nanoparticles in vivo and in vitro. *Toxicology letters* **2009**, *184*, (1), 18-25.
- 54  
55  
56  
57  
58  
59  
60



- 1  
2  
3 38. Nishanth, R. P.; Jyotsna, R. G.; Schlager, J. J.; Hussain, S. M.; Reddanna, P. Inflammatory  
4 responses of RAW 264.7 macrophages upon exposure to nanoparticles: role of ROS-NF $\kappa$ B signaling  
5 pathway. *Nanotoxicology* **2011**, *5*, (4), 502-516.
- 6 39. Panas, A.; Comouth, A.; Saathoff, H.; Leisner, T.; Al-Rawi, M.; Simon, M.; Seemann, G.;  
7 Dössel, O.; Mülhopt, S.; Paur, H.-R. Silica nanoparticles are less toxic to human lung cells when  
8 deposited at the air–liquid interface compared to conventional submerged exposure. *Beilstein*  
9 *journal of nanotechnology* **2014**, *5*, (1), 1590-1602.
- 10 40. Clark, I. A. How TNF was recognized as a key mechanism of disease. *Cytokine & growth*  
11 *factor reviews* **2007**, *18*, (3), 335-343.
- 12 41. Tse, B. W.; Scott, K. F.; Russell, P. J. Paradoxical roles of tumour necrosis factor-alpha in  
13 prostate cancer biology. *Prostate cancer* **2012**, *2012*.
- 14 42. Jing, Y.; Ma, N.; Fan, T.; Wang, C.; Bu, X.; Jiang, G.; Li, R.; Gao, L.; Li, D.; Wu, M. Tumor  
15 necrosis factor-alpha promotes tumor growth by inducing vascular endothelial growth factor. *Cancer*  
16 *investigation* **2011**, *29*, (7), 485-493.
- 17 43. Kedmi, R.; Ben-Arie, N.; Peer, D. The systemic toxicity of positively charged lipid  
18 nanoparticles and the role of Toll-like receptor 4 in immune activation. *Biomaterials* **2010**, *31*, (26),  
19 6867-6875.
- 20 44. Kateb, B.; Van Handel, M.; Zhang, L.; Bronikowski, M. J.; Manohara, H.; Badie, B.  
21 Internalization of MWCNTs by microglia: possible application in immunotherapy of brain tumors.  
22 *Neuroimage* **2007**, *37*, S9-S17.
- 23 45. Yang, Y.; Hu, Y.; Wang, Y.; Li, J.; Liu, F.; Huang, L. Nanoparticle delivery of pooled siRNA for  
24 effective treatment of non-small cell lung cancer. *Molecular pharmaceutics* **2012**, *9*, (8), 2280-2289.
- 25 46. Kettler, K.; Veltman, K.; van de Meent, D.; van Wezel, A.; Hendriks, A. J. Cellular uptake of  
26 nanoparticles as determined by particle properties, experimental conditions, and cell type.  
27 *Environmental toxicology and chemistry* **2014**, *33*, (3), 481-492.
- 28 47. Jin, H.; Heller, D. A.; Sharma, R.; Strano, M. S. Size-dependent cellular uptake and expulsion  
29 of single-walled carbon nanotubes: single particle tracking and a generic uptake model for  
30 nanoparticles. *Acs Nano* **2009**, *3*, (1), 149-158.
- 31 48. Dasargyri, A.; Hervella, P.; Christiansen, A.; Proulx, S. T.; Detmar, M.; Leroux, J.-C. Findings  
32 questioning the involvement of Sigma-1 receptor in the uptake of anisamide-decorated particles.  
33 *Journal of Controlled Release* **2016**, *224*, 229-238.
- 34 49. Aydar, E.; Onganer, P.; Perrett, R.; Djamgoz, M. B.; Palmer, C. P. The expression and  
35 functional characterization of sigma ( $\sigma$ ) 1 receptors in breast cancer cell lines. *Cancer letters* **2006**,  
36 *242*, (2), 245-257.
- 37 50. Cobos, E.; Entrena, J.; Nieto, F.; Cendan, C.; Pozo, E. Pharmacology and therapeutic potential  
38 of sigma1 receptor ligands. *Current neuropharmacology* **2008**, *6*, (4), 344-366.
- 39 51. Weichert, W.; Schmidt, M.; Gekeler, V.; Denkert, C.; Stephan, C.; Jung, K.; Loening, S.; Dietel,  
40 M.; Kristiansen, G. Polo-like kinase 1 is overexpressed in prostate cancer and linked to higher tumor  
41 grades. *The Prostate* **2004**, *60*, (3), 240-245.
- 42 52. Russo, M. A.; Kang, K. S.; Di Cristofano, A. The PLK1 inhibitor GSK461364A is effective in  
43 poorly differentiated and anaplastic thyroid carcinoma cells, independent of the nature of their  
44 driver mutations. *Thyroid* **2013**, *23*, (10), 1284-1293.
- 45 53. Steegmaier, M.; Hoffmann, M.; Baum, A.; Lénárt, P.; Petronczki, M.; Krššák, M.; Gürtler, U.;  
46 Garin-Chesa, P.; Lieb, S.; Quant, J. BI 2536, a potent and selective inhibitor of polo-like kinase 1,  
47 inhibits tumor growth in vivo. *Current Biology* **2007**, *17*, (4), 316-322.
- 48 54. Gilboa-Geffen, A.; Hamar, P.; Le, M. T.; Wheeler, L. A.; Trifonova, R.; Petrocca, F.; Wittrup, A.;  
49 Lieberman, J. Gene knockdown by EpCAM aptamer–siRNA chimeras suppresses epithelial breast  
50 cancers and their tumor-initiating cells. *Molecular cancer therapeutics* **2015**, *14*, (10), 2279-2291.
- 51 55. Shen, Y.; Li, J.; Nitta, M.; Futralan, D.; Steed, T.; Treiber, J. M.; Taich, Z.; Stevens, D.; Wykosky,  
52 J.; Chen, H.-Z. Orthogonal targeting of EGFRvIII expressing glioblastomas through simultaneous EGFR  
53 and PLK1 inhibition. *Oncotarget* **2015**, *6*, (14), 11751.
- 54  
55  
56  
57  
58  
59  
60

- 1  
2  
3 56. Malhotra, M.; Tomaro-Duchesneau, C.; Saha, S.; Prakash, S. Systemic siRNA delivery via  
4 peptide-tagged polymeric nanoparticles, targeting PLK1 gene in a mouse xenograft model of  
5 colorectal cancer. *International journal of biomaterials* **2013**, *2013*.  
6  
7 57. Hutmacher, D. W. Biomaterials offer cancer research the third dimension. *Nature materials*  
8 **2010**, *9*, (2), 90-93.  
9  
10 58. Pampaloni, F.; Reynaud, E. G.; Stelzer, E. H. The third dimension bridges the gap between  
11 cell culture and live tissue. *Nature reviews Molecular cell biology* **2007**, *8*, (10), 839-845.  
12  
13 59. Chambers, K. F.; Mosaad, E. M.; Russell, P. J.; Clements, J. A.; Doran, M. R. 3D cultures of  
14 prostate cancer cells cultured in a novel high-throughput culture platform are more resistant to  
15 chemotherapeutics compared to cells cultured in monolayer. *PloS one* **2014**, *9*, (11), e111029.  
16  
17 60. Leong, D. T.; Ng, K. W. Probing the relevance of 3D cancer models in nanomedicine  
18 research. *Advanced drug delivery reviews* **2014**, *79*, 95-106.  
19  
20  
21  
22  
23  
24  
25  
26  
27  
28  
29  
30  
31  
32  
33  
34  
35  
36  
37  
38  
39  
40  
41  
42  
43  
44  
45  
46  
47  
48  
49  
50  
51  
52  
53  
54  
55  
56  
57  
58  
59  
60

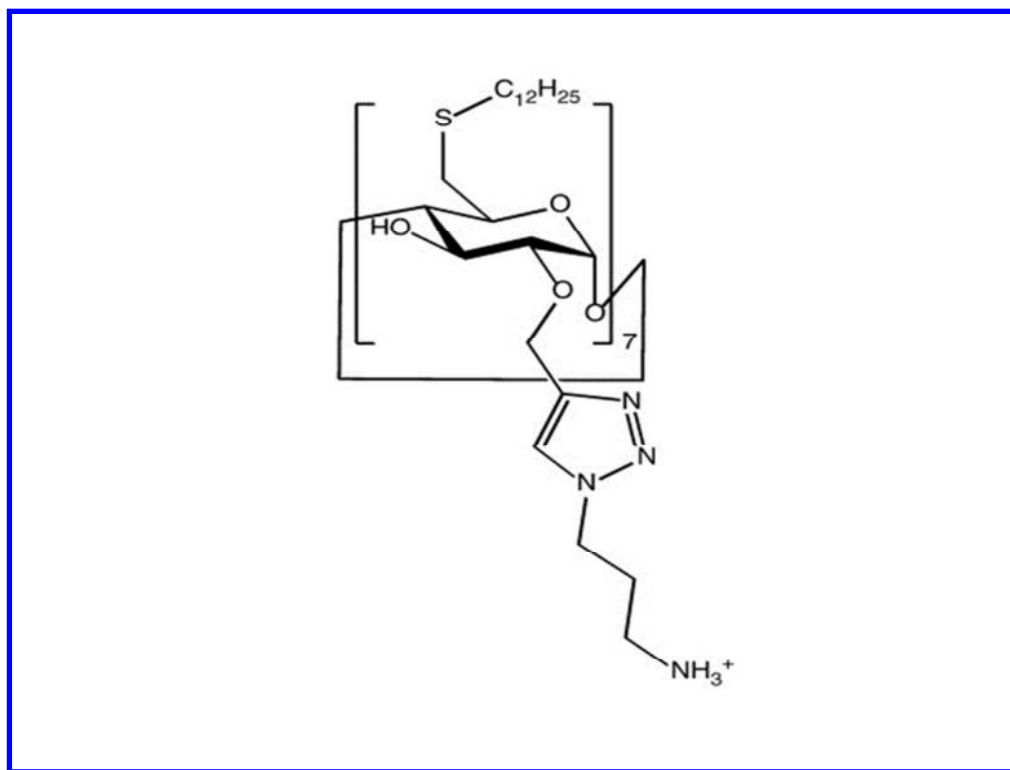


Figure 1

254x190mm (96 x 96 DPI)

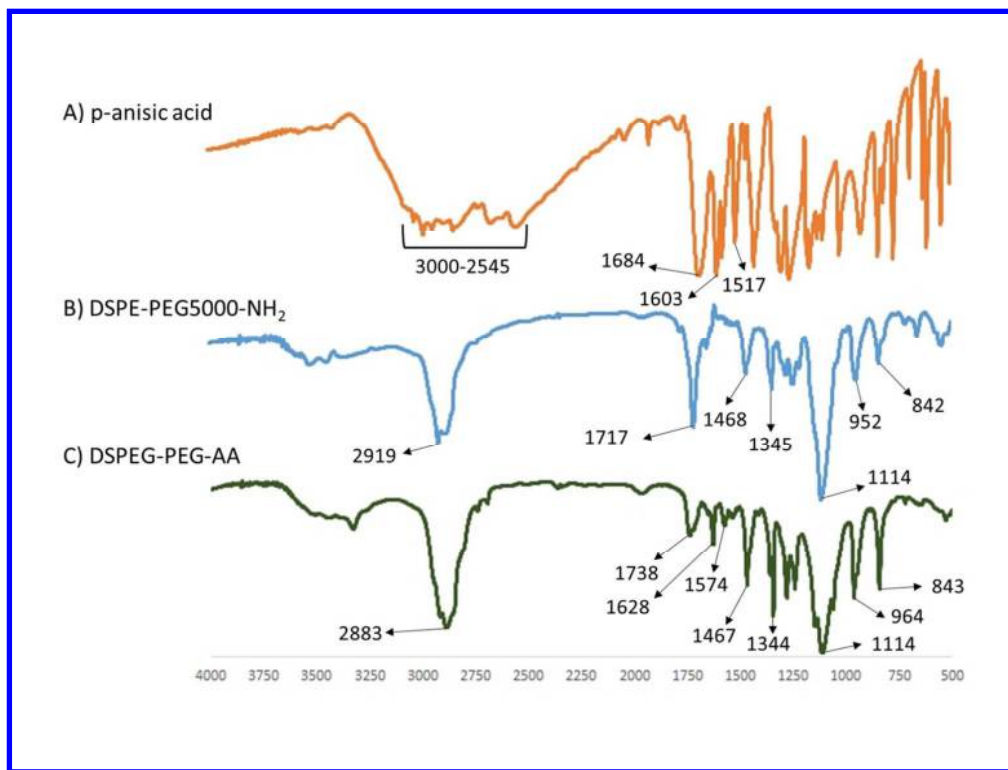


Figure 3

355x266mm (96 x 96 DPI)

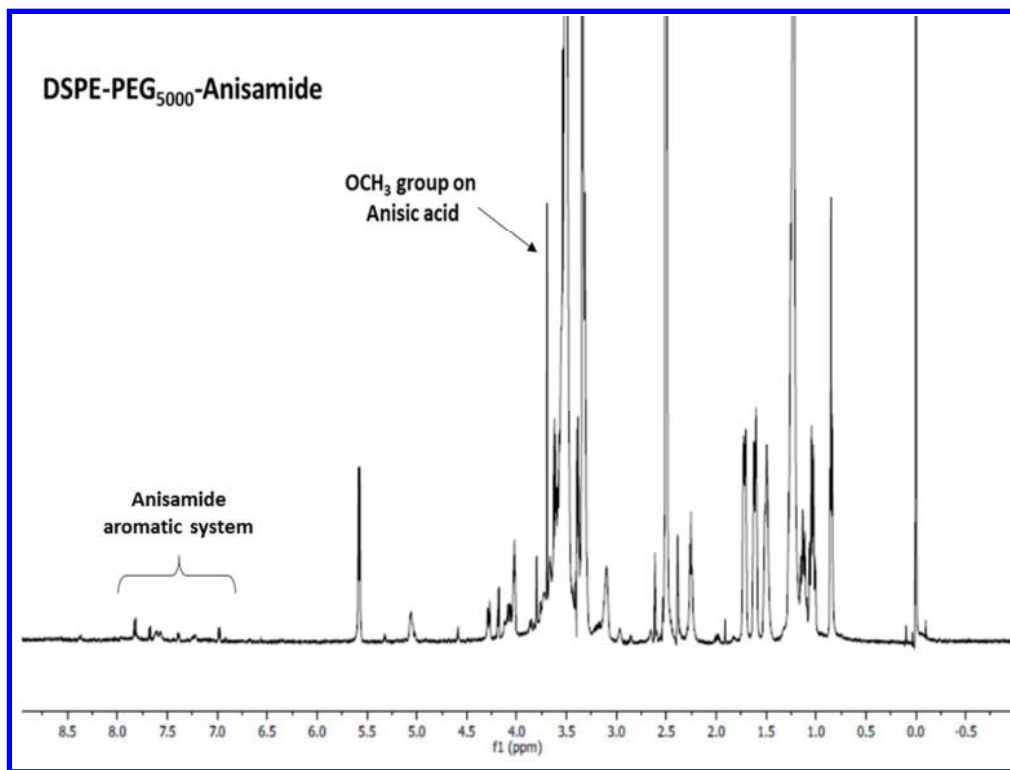


Figure 2

254x190mm (96 x 96 DPI)

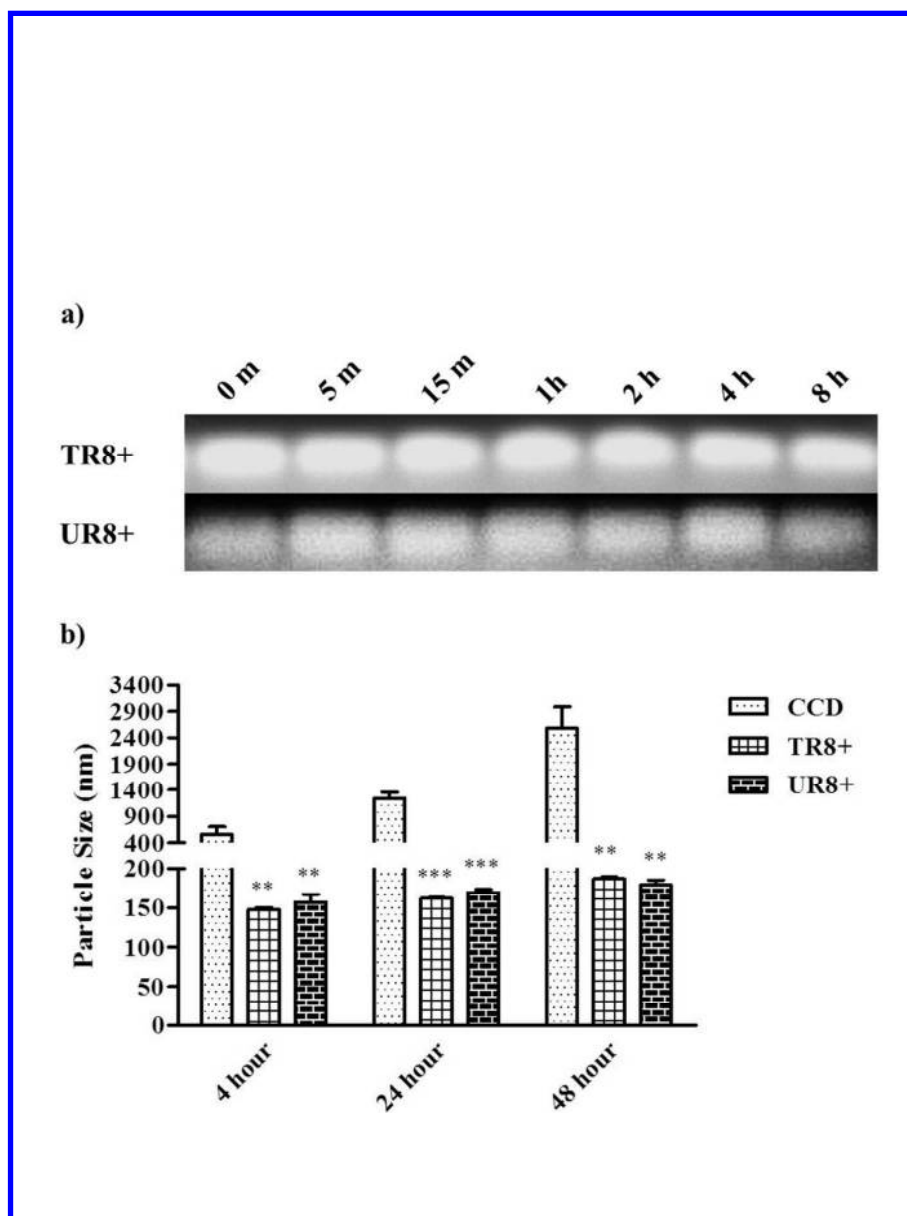


Figure 4

266x355mm (96 x 96 DPI)

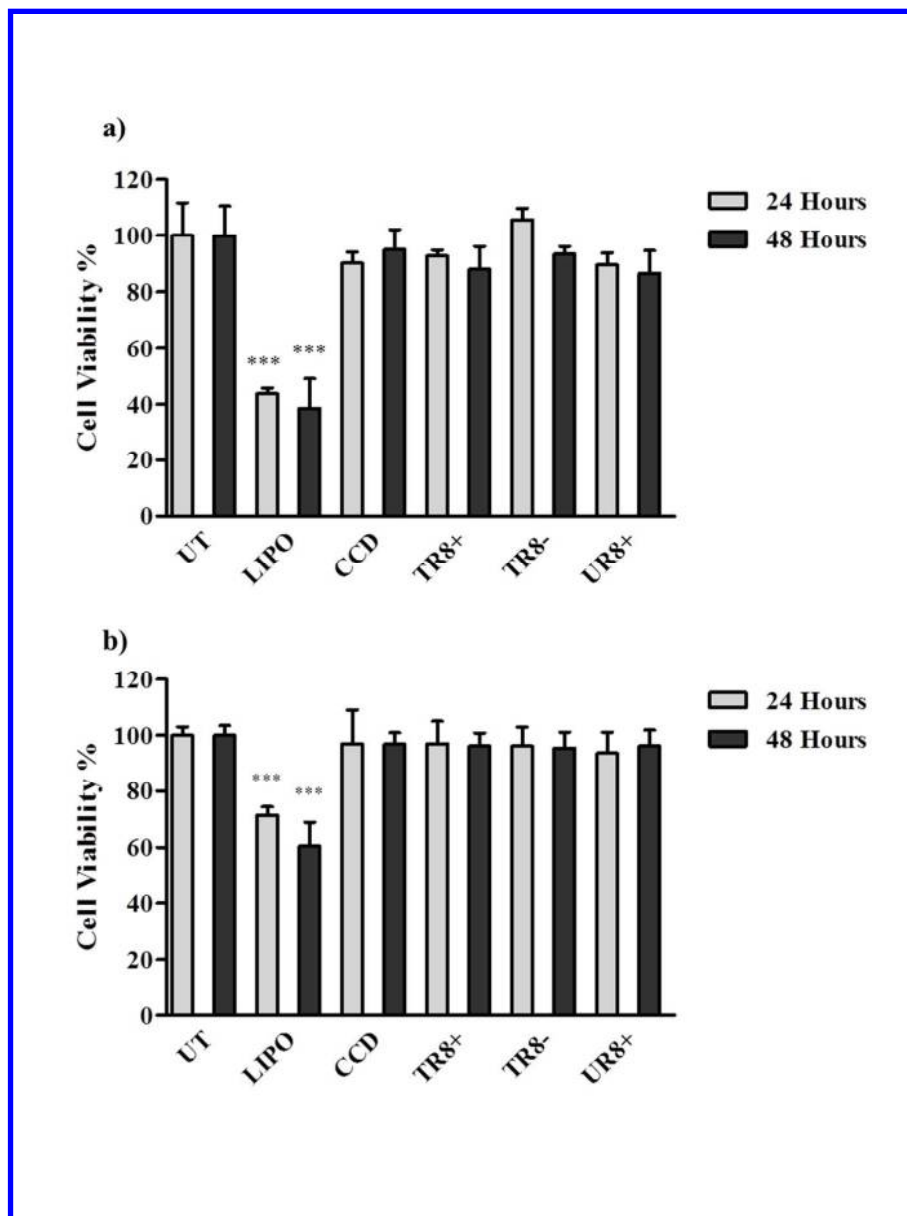


Figure 5

266x355mm (96 x 96 DPI)

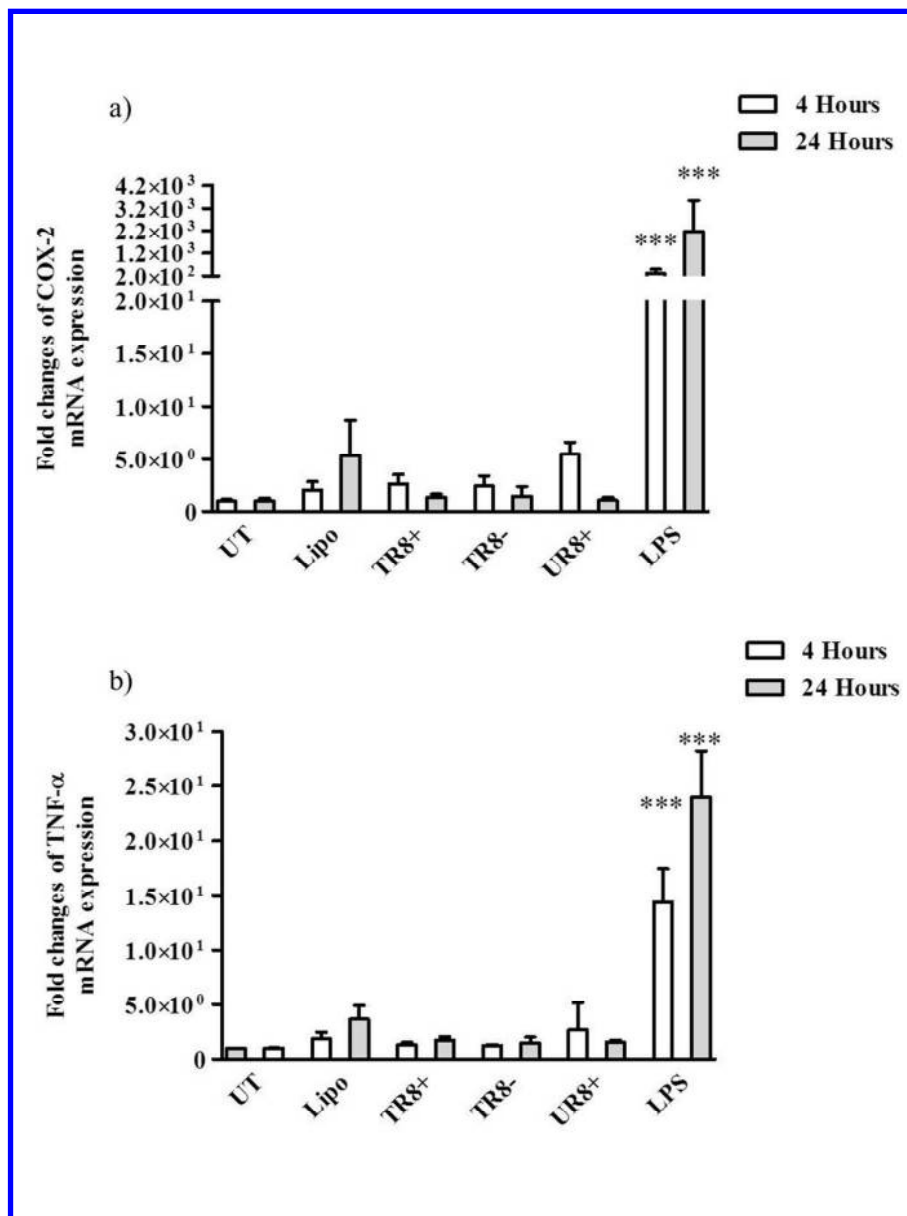


Figure 6

266x355mm (96 x 96 DPI)



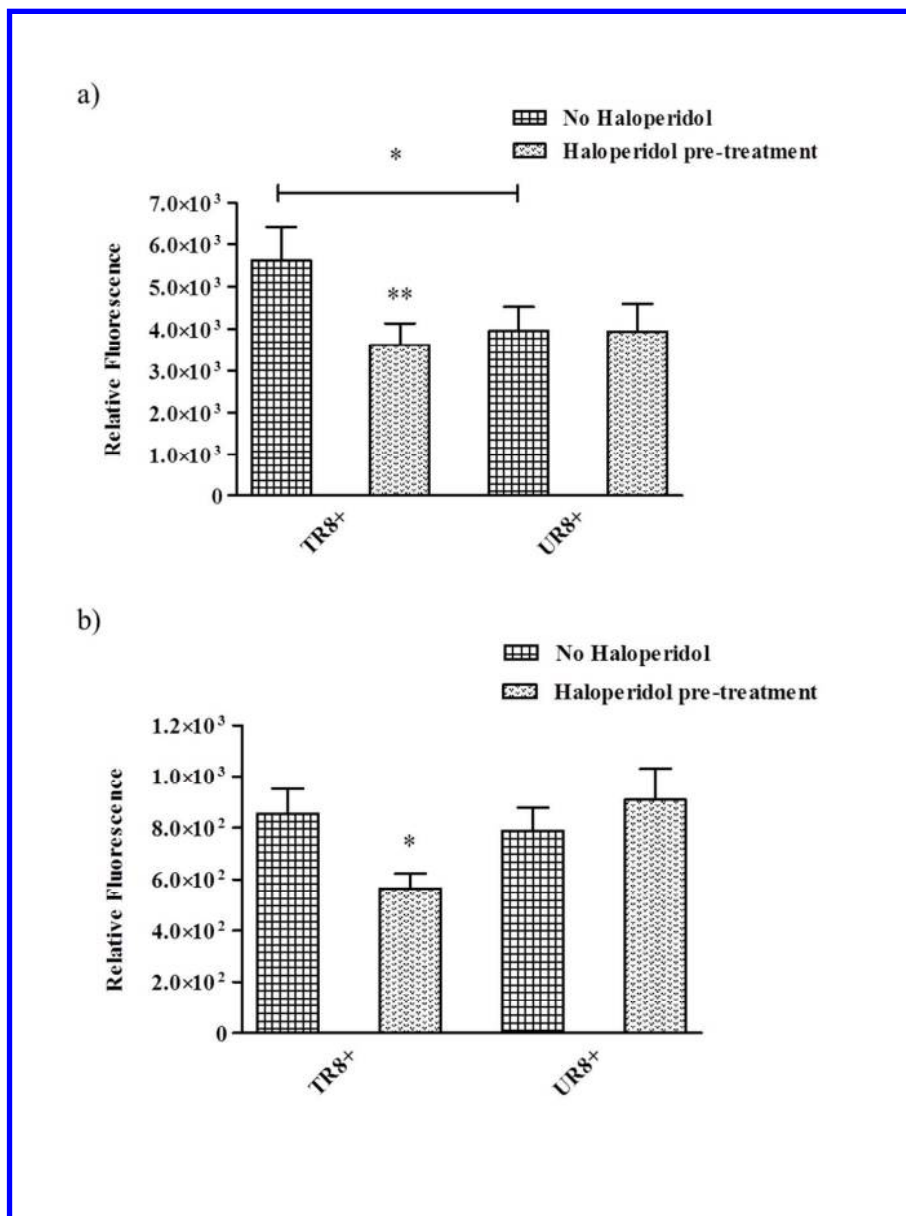


Figure 7

266x355mm (96 x 96 DPI)

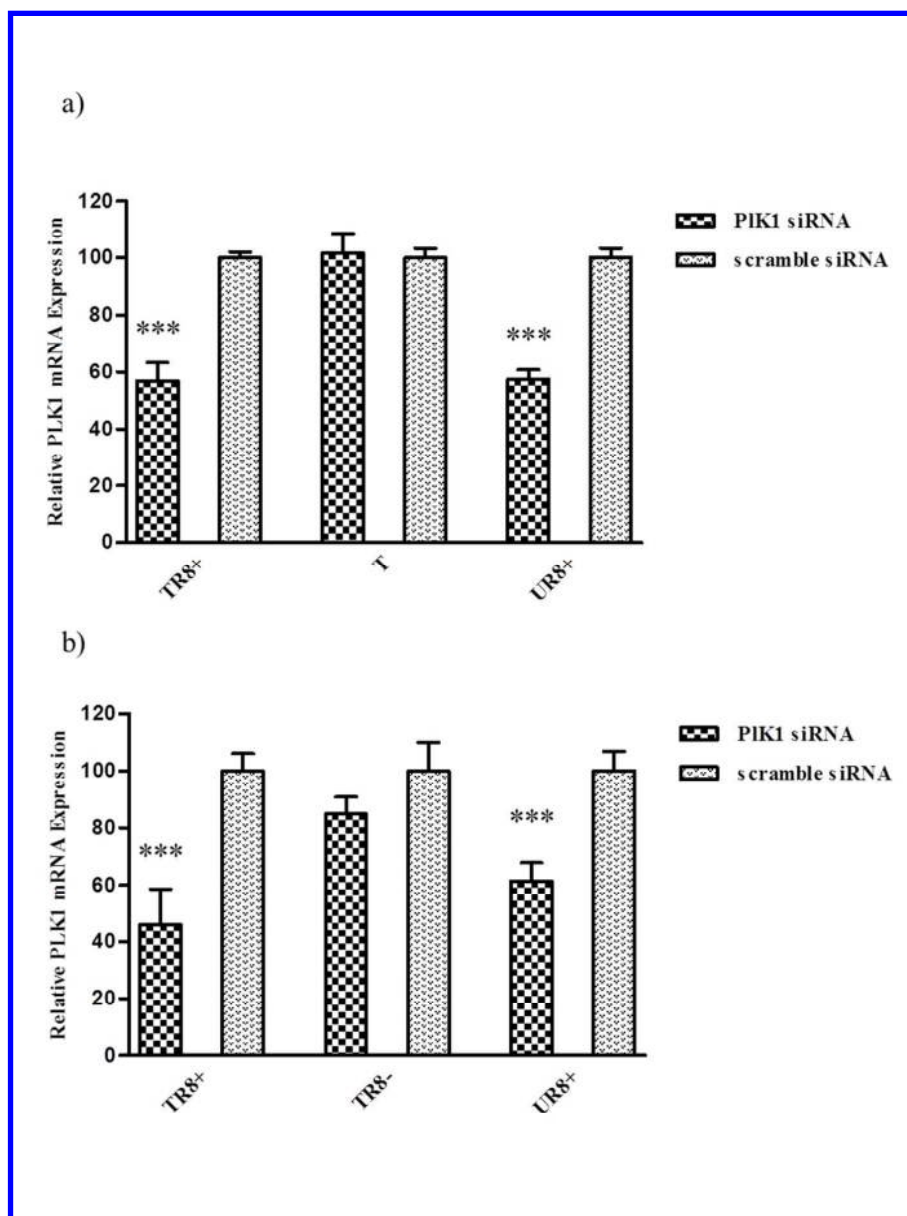


Figure 8

266x355mm (96 x 96 DPI)

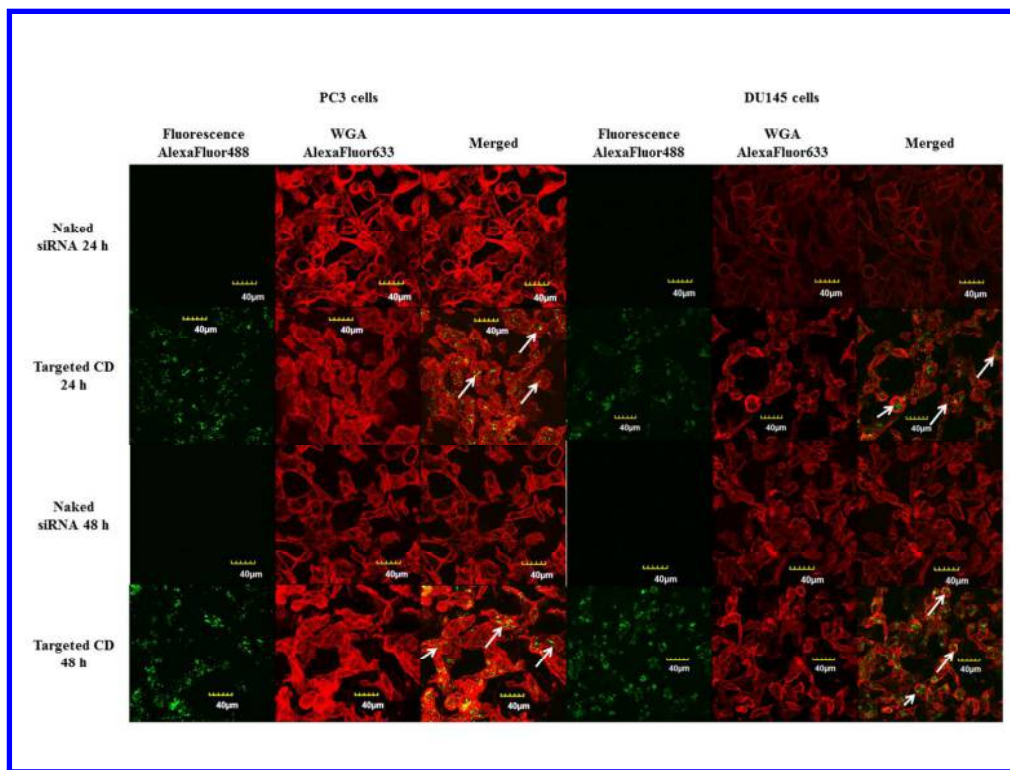


Figure 9

355x266mm (96 x 96 DPI)

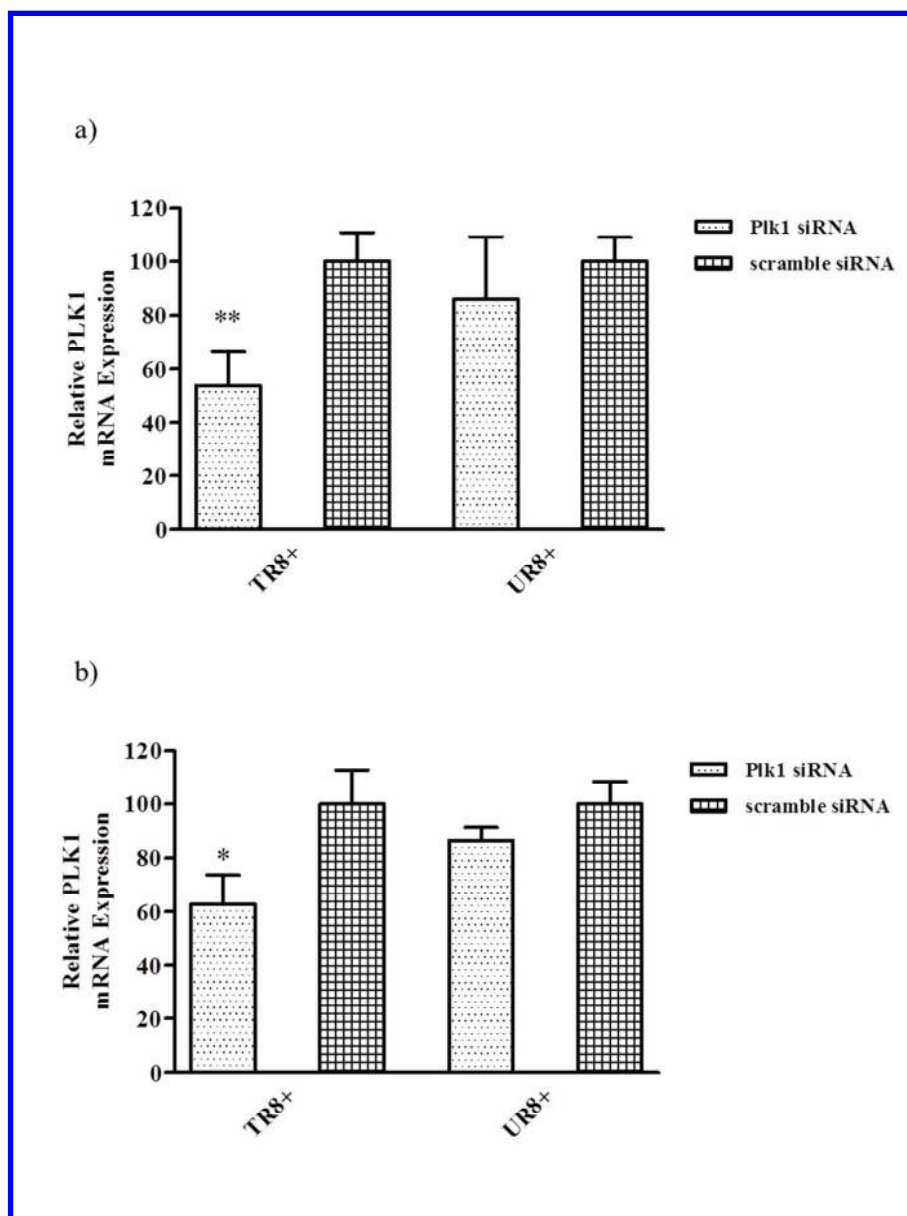
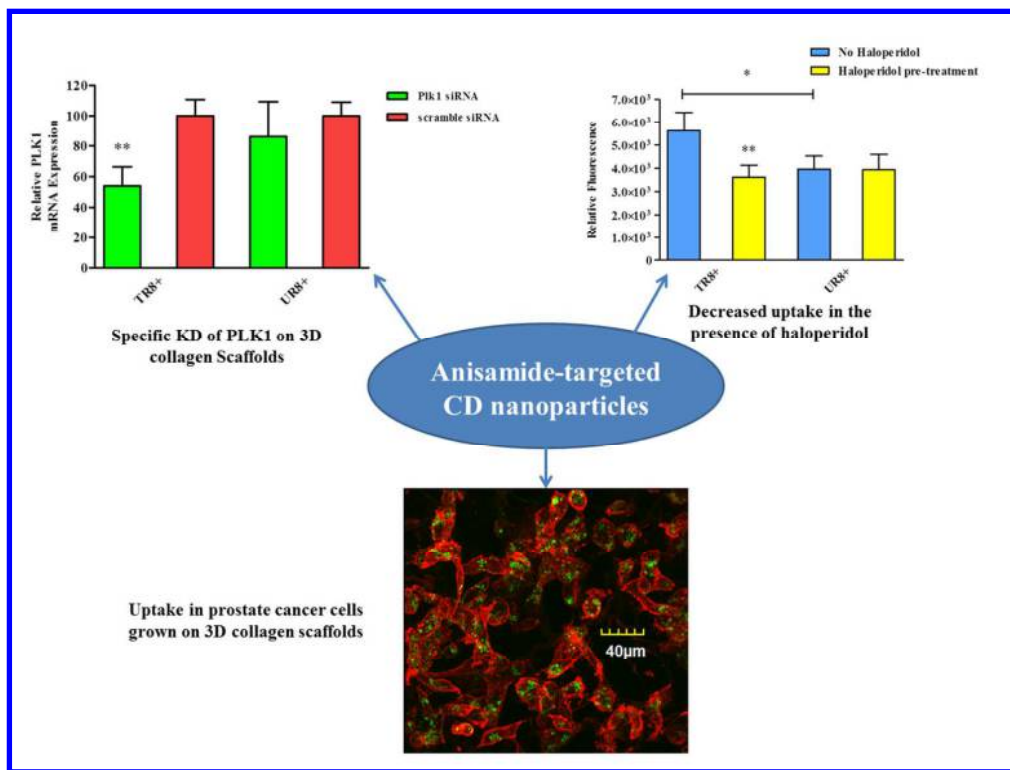


Figure 10

266x355mm (96 x 96 DPI)



355x266mm (96 x 96 DPI)